Paleomagnetic Data Bearing on Vertical Axis Rotation of the Rio del Oso dike swarm, Western Española Basin, New Mexico

M.S. Petronis, R.V. Trujillo, J. Lindline, and J.P. Zebrowski

New Mexico Geology, v. 42, n. 2 pp. 61-78, Online ISSN: 2837-6420.
https://doi.org/10.58799/NMG-v42n2.61

New Mexico Bureau of Geology & Mineral Resources
New Mexico Institute of Mining & Technology
801 Leroy Place
Socorro, NM 87801-4796

https://geoinfo.nmt.edu

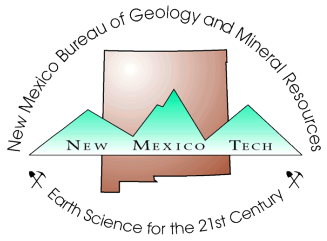

This page is intentionally left blank to maintain order of facing pages.

Paleomagnetic data bearing on vertical axis rotation of the Rio del Oso dike swarm, western Española Basin, New Mexico

Petronis, M.S.[1], *Trujillo, R.V.*[1, 2], *Lindline, J.*[1], and *Zebrowski, J.P.*[1]

[1]Environmental Geology, Natural Resources Management Department, New Mexico Highlands University, P.O. Box 9000, Las Vegas, NM 87701
[2]New Mexico Environment Department, Air Quality Bureau, 525 Camino de los Marquez, Suite 1, Santa Fe, New Mexico, 87505-1816

Abstract

The Española Basin is one of a series of interconnected, asymmetrical basins in the Rio Grande rift that includes a number of north- and northeast-striking faults that accommodated block tilting and basin subsidence. The western margin of the Española Basin, in particular, is characterized by a greater than 17-km wide zone of normal and oblique-slip faults. To clarify the involvement of block rotation in the tectonic evolution of the Española Basin, we carried out a paleomagnetic study of mafic intrusions (Rio del Oso dike swarm) that are genetically related to regionally extensive basalt flows of the mid-Miocene Lobato Formation. The primary hypothesis tested was that these intrusions experienced some degree of vertical axis rotation associated with mid-Miocene to recent continental rifting. In situ paleomagnetic results from forty-two sites yield a group mean declination (D) of 344.0°, an inclination (I) of 41.1°, α_{95} of 6.1°, and *k* of 14.1. The group mean result is discordant to the <10 Ma pole of D=356.0°, I=54.4°, α_{95} = 3.3° with a statistically significant inferred rotation (R) of -12.0°± 7.2° and flattening of +13.3° ± 5.5° relative to the <10 Ma pole field direction. These discordant results indicate that a modest degree of counter-clockwise vertical axis rotation occurred in this region, which is likely associated with Rio Grande rifting north of the Jemez Mountains. It is possible that oblique motion along the Santa Clara fault and/or the Cañada del Almagre fault facilitated the vertical axis rotation. The results from this study imply that vertical axis rotation is common to extensional rift systems and should be considered when modeling continental extension.

Introduction

The Rio Grande rift is a roughly north-south trending intracratonic rift that separates the over thickened and relatively undeformed continental crust of the Colorado Plateau on the west from the stable craton of the Great Plains to the east (Kelley, 1977; Aldrich and Dethier, 1990; Chapin and Cather, 1994). The rift extends south from about Leadville, Colorado and merges with the eastern Basin and Range Province of eastern Arizona, New Mexico, and northern Mexico (Fig. 1). Characteristics of the rift include high heat flow, structurally-controlled basins, crustal deformation, and Cenozoic to Holocene silicic to mafic volcanism. The high heat flow is attributed to upper mantle asthenospheric upwelling and thermal lithospheric erosion (Seager and Morgan, 1979; Morgan et al., 1986; Wilson et al., 2005). In northern New Mexico and southern Colorado, the structural manifestation of the rift is a series of right-stepping, asymmetric fault-bounded en echelon basins with extension increasing southward (Kelley, 1982). From north to south, these are the upper Arkansas River Basin, San Luis Basin, Española Basin, Albuquerque Basin, and the southern Rio Grande Basin (Fig. 1). Rift deformation from ca. 30 to 20 Ma resulted in a broad zone of distributed extension along low-angle faults, crustal doming, widespread magmatic activity, and accumulation of sediment in intrarift basins (Chapin, 1988; Prodehl and Lipman, 1989). Between ca. 20 and 10 Ma, the rate of extension accelerated with rifting restricted to a narrower zone and characterized by high-angle normal faulting and the onset of alkalic mafic magmatism (Golombek et al., 1983; Prodehl and Lipman, 1989; Baldridge et al., 1991). The rate of extension has decreased in the last 5 Ma, but the rift remains seismically and magmatically active (Grauch et al., 2017). We hypothesize that Rio Grande rift faulting in the northwestern Española Basin was accommodated by extension and counter-clockwise rotation of fault-bounded crustal blocks. To assess this hypothesis, we obtained paleomagnetic data from Miocene mafic intrusions of the Rio del Oso dike swarm (Koning et al., 2007) in the western Española Basin. We also conducted petrographic examination of the studied intrusions to confirm their affinity to the regionally extensive extrusive basalts of the Lobato Formation.

Geologic and tectonic history of the Española Basin

The Española Basin, located in north-central New Mexico, is bordered by the Nacimiento uplift to the west and the Sangre de Cristo Mountains to the east (Fig. 1). The Española Basin likely developed by about 26 Ma and was initially ~3 km deep during the Oligocene (Golombek et al., 1983). Renewed tectonism during the early Miocene resulted in localized faulting that led to significant accumulations of sediment in the north and central parts of the basin with thicknesses reaching up to 5 km (Aldrich, 1986; Golombek et al., 1983). The rift-basin deposits are collectively referred to as the Santa Fe Group. At approximately 10 Ma, basin subsidence slowed and sediment aggradation ensued, resulting in thick deposits of the Santa Fe Group within the Española Basin (Aldrich and Dethier, 1990). In addition, between 15 Ma and 14 Ma, volcanism occurred at the northwestern edge of the basin (Aldrich and Dethier, 1990) along the Jemez Lineament, a complex suture zone between the Mesoproterozoic Yavapai and the Mazatzal lithospheric provinces that facilitated volcanism and tectonism near the Jemez

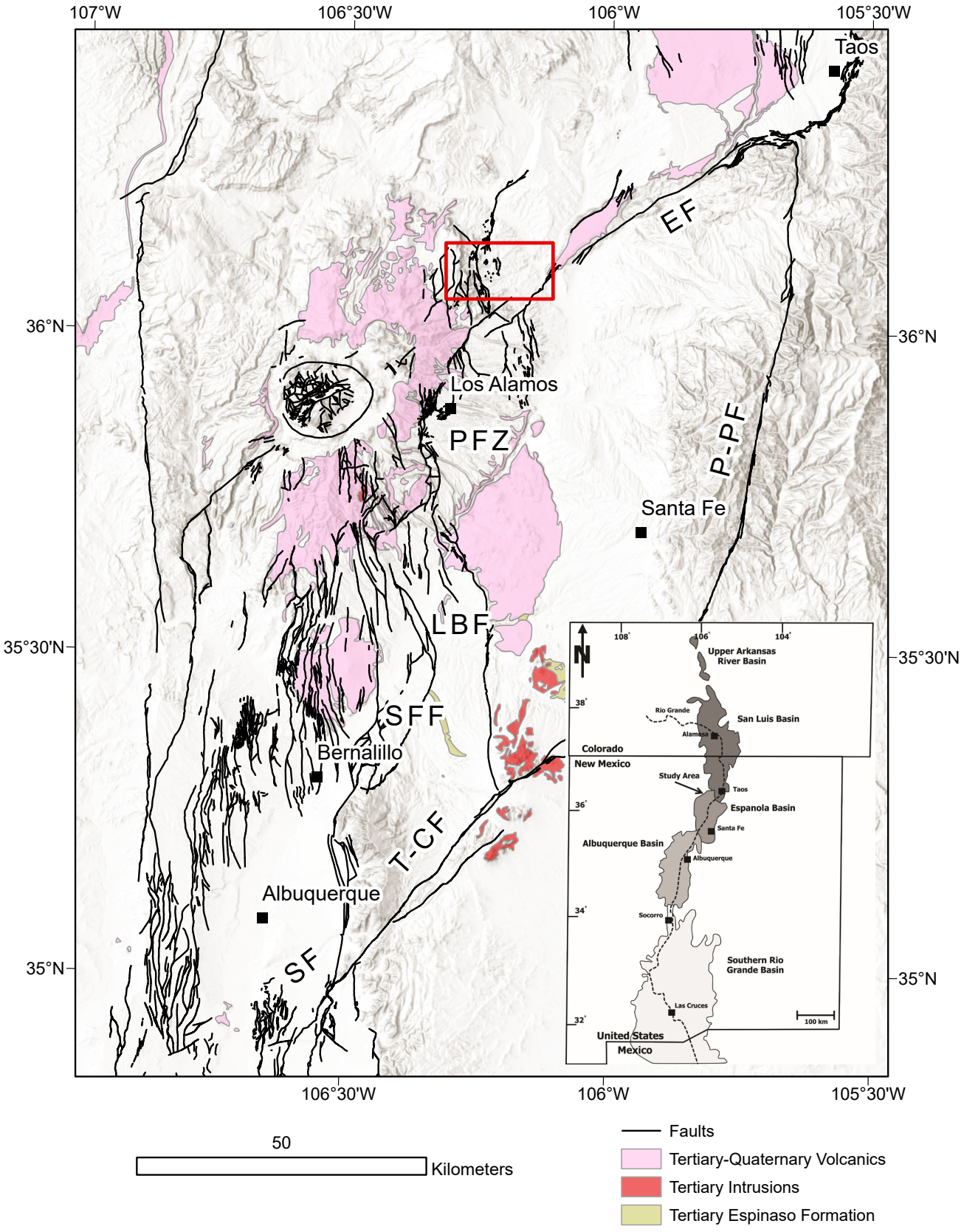

Figure 1. Inset: General sketch map depicting the Rio Grande rift and related sub-basins throughout southern Colorado, New Mexico, and Mexico (modified from Grauch and Bankey, 2003). Tectonic map of part of northern New Mexico showing the location of the the Española block. T-CF—Tijeras-Cañoncito fault zone; PFZ—Pajarito fault zone; EF—Embudo fault zone; P-PF—Picuris-Pecos fault zone; LBF—La Bajada fault; SFF—San Felipe fault; SF—Sandia fault. Red rectangle indicates area shown in the Figure 2 map. Location map modified from http://cires.colorado.edu/science/groups/sheehan/projects/riogrande/images/faq2.jpg. Faults on tectonic map are from the U.S. Geological Survey Quaternary fault and fold database (http://gldims.cr.usgs.gov); geologic units are from NMBGMR (2003).

Mountains and locally throughout the Rio Grande rift (Aldrich, 1986; Wolff et al., 2005). Jemez Mountain volcanism began with the eruption of the Lobato Formation basalts from numerous vents until approximately 10 Ma. At ~9 Ma, volcanism slowed drastically with only minor Lobato volcanism continuing until ~7 Ma (Aldrich and Dethier, 1990). The end of basaltic volcanism in this area is thought to be related to a change in the regional stress field. This switch is evident throughout western North America and has been inferred to reflect reorganization of North American-Pacific plate boundary conditions (Golombek et al., 1983; Prodehl and Lipman, 1989; Atwater and Stock, 1998).

Lobato Formation Basalts

The Lobato Formation basalts are the oldest unit of the Polvadera Group, which crops out on the northern to eastern flanks of the Jemez Mountains and forms prominent mesas throughout the area (Smith, 1938; Koning et al., 2005). The Lobato Formation consists of multiple flows, associated cinder deposits, and intrusive rocks (dikes and stocks) of primarily olivine basalt that yield K-Ar age determinations ranging from 14.05 ± 0.33 Ma to 7.6 ± 0.4 Ma (Dalrymple and Hirooka, 1965; Bachman and Mehnert, 1978; Luedke and Smith, 1978; Baldridge et al., 1980; Manley and Mehnert, 1981; Aldrich, 1986; Gardner et al., 1986) with a voluminous phase of volcanism occurring between 10.8 ± 0.3 Ma to 9.1 ± 0.2 Ma (Gardner et al., 1986). Lobato volcanism and associated intrusive magmatism occurred concurrently and was likely driven by tectonic activity associated with Rio Grande rifting. Across the region, eruption of the Lobato basalts likely occurred from at least four vents producing a number of large shield cones and possibly fissure vents. Individual flows are 2 to 5 meters thick, and interfinger locally with clastic sediments of the Santa Fe Group (Baldridge et al., 1980; Dethier and Manley, 1985). Intrusive bodies occur locally across the Española Basin, with a relatively large dike set (the Rio del Oso dike swarm) located in the Chili 7.5' quadrangle (Koning et al., 2005). Intrusions associated with Lobato Formation basalts contain 1 to 2 mm crystals of plagioclase, olivine, and augite.

Geology of the Chili quadrangle

Dikes in the Rio del Oso swarm were studied in the northwest corner of the Chili quadrangle, which lies north of the intersection of the Jemez Lineament and the western margin of the Española Basin in Oso Arroyo just west of Chili, New Mexico (Fig. 1). The Chili quadrangle is situated in a structurally diverse part of the basin that exhibits a complex brittle kinematic history (Koning et al., 2005; Fig. 1). A variety of rift-related geologic features as old as middle Miocene are well-exposed in the area. These features include an array of normal and strike-slip faults, a relatively complete sequence of middle to upper Miocene and Pliocene rift-basin sediments, upper Miocene basaltic intrusions and lava flows, and a well-preserved set of Quaternary terraces (Koning et al., 2005). Major structures in the area include the Santa Clara Fault, a northeast-southwest striking, east-dipping sinistral oblique-slip fault located in the southern part of the Chili quadrangle; the Cañada del Amagre fault, which strikes north to northwest with dextral offset; and the dextral Guaje Mountain fault (Aldrich and Dethier, 1990; Koning et al., 2005). The Cañada del Amagre fault and the Guaje Mountain fault have comparatively large components of strike-slip relative to dip-slip motion, and suggest that the horizontal component of displacement along these faults may be related to counterclockwise rotation between structural blocks (Aldrich and Dethier, 1990) as demonstrated in numerous tectonic settings (Otofuji et al., 1985, Hudson et al., 2004, Petronis et al., 2002).

We collected samples from dikes in the Rio del Oso swarm (Fig. 2), which trend generally north-south and show both a right- and left-stepping en echelon geometry. En echelon dike systems are often argued to be interconnected at depth (e.g., Baer, 1991). Anderson (1951) proposed that dike segmentation may be attributed to rotation of the minimum principle stress ($\sigma 3$) toward the surface during magma intrusion. We sampled at least eight distinct intrusions at four locations spread over an ~4.8 km^2 area, although the number of sampled intrusions is a minimum estimate because of difficulty tracing individual dikes along strike. The dikes intrude Miocene Santa Fe Group deposits and form prominent ridges across the landscape (Fig. 3). The dikes have been dated by the K-Ar method to yield age estimates of 9.7 ± 0.3 Ma, 10.7 ± 0.3 Ma, and 10.6 ± 0.3 Ma (Baldridge et al., 1980). Likely correlative lava flows from the area have a similar mineralogy as the intrusions and yield age determinations that range from 9.6 ± 0.2 Ma to 12.4 Ma (Dethier et al., 1986, Dethier and Manley, 1985).

No detailed paleomagnetic studies have been conducted on the dikes in this area. In northern New Mexico, several paleomagnetic studies (Brown and Golombek, 1985, 1986; Salyards et al., 1994; Harlan and Geissman, 2009; Petronis and Lindline, 2011) have reported data supporting the presence of statistically significant vertical axis block rotations or lack thereof associated with Rio Grande rift extension (Table 1). Brown and Golombek (1986) reported counter-clockwise (CCW) rotation of intrusive rocks of the Ortiz porphyry belt within the Española Basin that yielded an apparent CCW rotation of –17.8° ± 11.4°. They postulated that the CCW rotations were the result of left-lateral slip along major faults bounding the rift (Muehlberger, 1979; Brown and Golombek, 1986). Salyards et al. (1994) conducted a paleomagnetic study within the Española Basin that concluded that the north-central Rio Grande rift is not rotating as a single unit, but rather as a number of smaller, independently CCW-rotating structural blocks. Aldrich and Dethier (1990) suggested that due to the large strike-slip components on the major faults in the Española Basin, it is probable that fault-bounded blocks have, and continue to undergo,

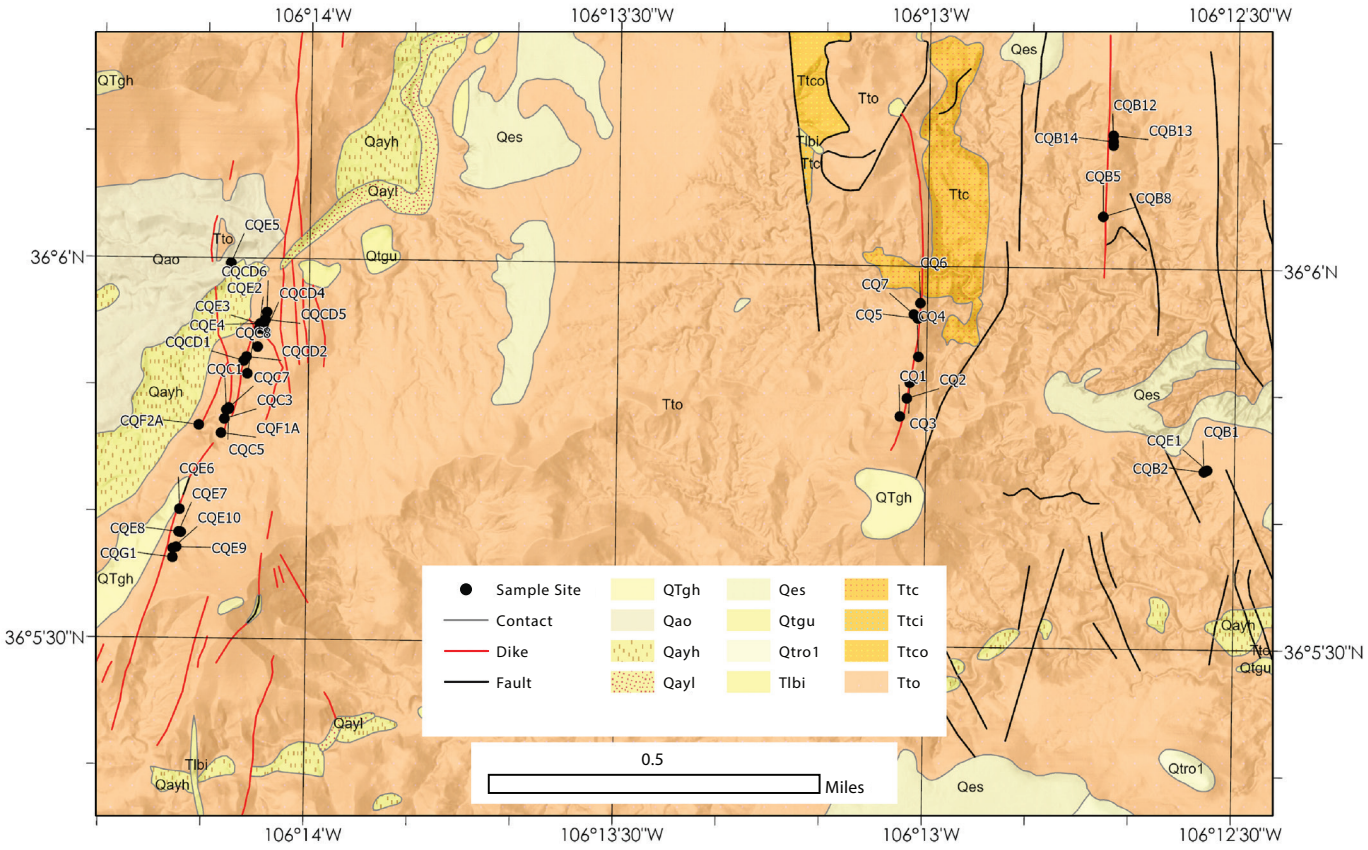

Figure 2. Geologic map (Koning, et al., 2005) of the area where the Rio del Oso dikes were sampled. See Table 2 for the paleomagnetic results from these sites.

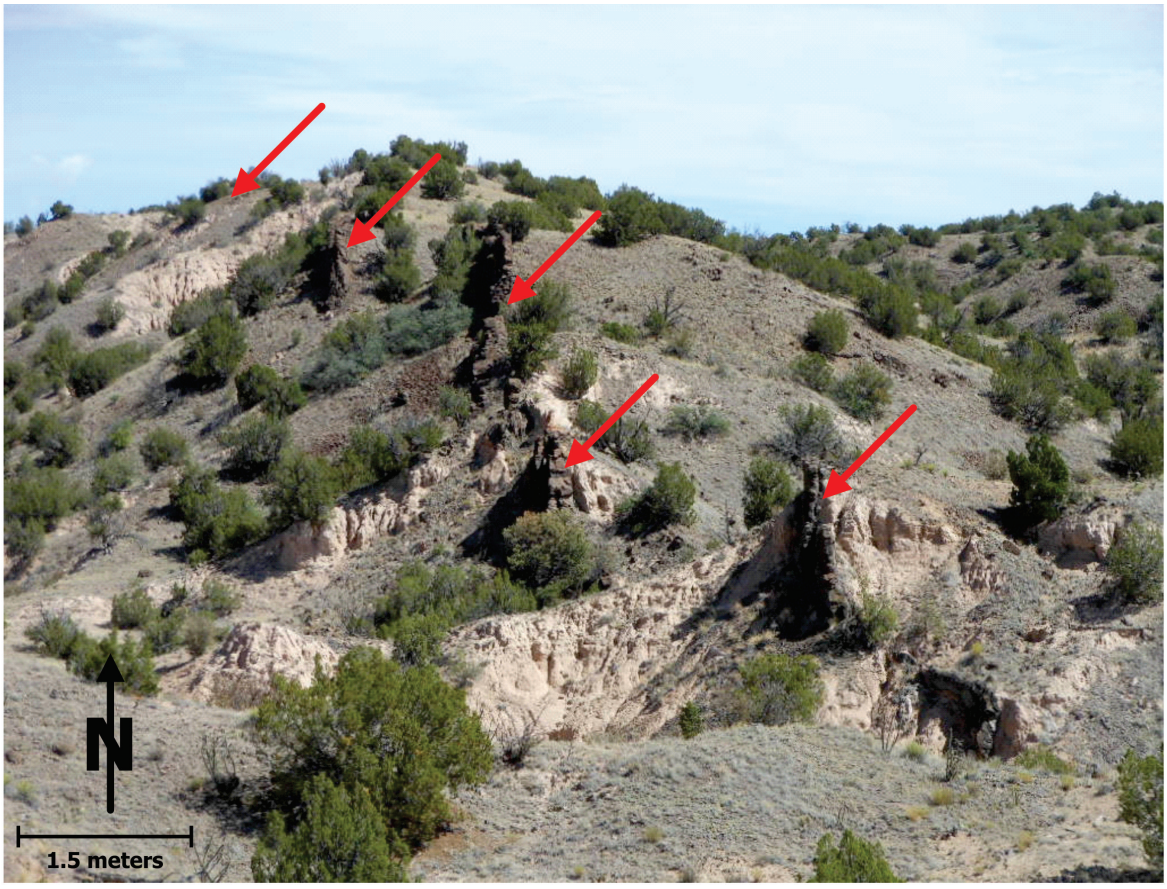

Figure 3. Field photograph of one of the studied dikes (red arrows) showing the common en echelon outcrop pattern.

significant vertical-axis rotation. Petronis and Lindline (2011) conducted a paleomagnetic study of an apparent monoclinal fold within the Lobato Formation basalts adjacent to the Santa Clara fault in the Chili quadrangle. They concluded, based on the results of a paleomagnetic fold test (Cox and Doell, 1960), that the lava flowed across a paleoescarpment into a paleovalley that existed adjacent to the Santa Clara Fault, with no evidence of vertical-axis rotation. Outside of the Española Basin, other studies have shown either negligible or statistically significant clockwise (CW) rotations. For example, Harlan and Geissman (2009) presented paleomagnetic data from in situ Tertiary intrusions and tilt-corrected volcaniclastic strata of the Oligocene Espinaso Formation, which yielded results indistinguishable from the 30 Ma reference direction for the study area. However, they argue that if an alternative reference direction is used, minor CCW rotation (–6.6° ± 5.8°) is possible. These studies show a complex image of crustal block rotation accompanying rift extension in northern New Mexico and likely in other rift systems world-wide. Many paleomagnetic rotation estimates from the rift and surrounding areas are based on small sample populations, and it is unclear whether results from individual studies adequately sampled paleosecular variation. The purpose of this study is to better assess possible block rotation in the western Española Basin and thus contribute to a better understanding of the kinematics of Rio Grande rift extensional dynamics.

Table 1: Paleomagnetic rotation estimates for the Española Basin and surrounding region.

Paleomagnetic Studies	R± Δ R	F± Δ F	Source
CF: Chamita Formation	-11.5° ± 5.3°	3.9° ± 5.1°	6,7
SFES: Chamita Formation	-11.1° ± 5.1°	N/A	1
SFTE: Tesuque Formation-Nambe Member	-0.6° ± 5.1°	N/A	1
SFAS: Tesuque Formation Skull Ridge Member	-5.0 ± 6.0°	N/A	1
SFSR: Nambe Member	-8.3° ±7.2°	N/A	1
SFCA: Chamita Formation	-28.5° ± 11.1°	N/A	1
CRV: Cerros del Rio Volcanics	-19.2° ± 14.8°; -14.7° ± 9.8°	-6.9° ± 6.9°; 2.5° ± 5.9°	2,3
TF: Tesuque Formation	-18.5° ± 5.8°	4.0° ± 5.5°	4,6
CH3: Cerillos Hills–Ortiz Mounatins	1.8 °± 6.4°	3.0° ± 4.0	3
*< 10 Ma Lobato Basalt	7.2°± 14.3	0.9°±12.9°	2
*VR: Valles Rhyolite	8.0° ± 9.2°	1.5°± 8.4	5,6
*TSF: Tschicoma Formation	19.4°±13.9°	2.7°±13.2	2
*PCF: Paliza Canyon Formation	11.9°±17.4°	1.6°±16.0°	2
CQ: Chili Quadrangle Basaltic Dikes	-12.0°± 7.2°	+13.3°± 5.5°	This study

EXPLANATION: Paleomagnetic studies are the site locations with published paleomagnetic data (* indicates site not shown on Figure 10B); R is the rotation and ΔR is the error (after Demarest, 1983); F is the flattening and ΔF is the error (after Demarest, 1983). 1, Salyards et al., 1994; 2, Brown and Golombek, 1985; 3, Harlan and Geissman, 2009; 4, Barghoorn, 1981; 5, Singer and Brown, 2002; 6, Brown and Golombek ,1986; 7, MacFadden, 1977.

Methods

Field and laboratory sampling methods

Field sampling began in October 2010 with eight to ten drill-core samples collected at fifty-seven sites (Fig. 2) across the area using a modified Echo 280E gasoline-powered drill with a non-magnetic diamond tip drill bit. All samples were oriented using a magnetic compass and, when possible, a sun compass. At each site, independent core samples were drilled along the margins and/or across the center of the dikes with the total number of samples collected at each site dependent on the level of exposure. All core samples were cut into 2.2 cm by 2.5 cm cylinder specimens using a diamond tipped, non-magnetic saw blade at New Mexico Highlands University's Rock Processing laboratory, with up to three specimens per core sample obtained. Drill site locations were precisely located using a Garmin GPS 60Csx (WGS84 datum). To characterize the magnetic mineralogy, we conducted a suite of laboratory experiments with the goal of identifying the magnetic phases carrying the remanence, and the overall ability of these rocks to faithfully record an ambient magnetic field. Equipment used included an AGICO JR6A dual-speed spinner magnetometer, ASC D-2000 (static) alternating field demagnetizer, and home-built and ASC Scientific (Model IM-10-30) static impulse magnets capable of 1 to 3 Tesla peak fields. All susceptibility and Curie point experiments were measured with an AGICO MFK1-A kappabridge susceptibility meter, with a CS4 high-temperature attachment at the New Mexico Highlands University Paleomagnetic-Rock Magnetic laboratory.

Rock magnetic experiments

Curie point experiments were used to establish the dominant magnetic mineral phase(s) present in the sample and to define the composition of the titanomagnetite phase(s). The procedure was performed in steps of heating and cooling from 25°C to 700°C and back to 40°C in an argon atmosphere to minimize oxidation of the sample, using a CS4 furnace attachment for the MFK1-A at a rate of ~14°C/min. The inflection point method (Tauxe, 1998) and Hopkinson Peak method (Hopkinson, 1889; Moscowitz 1981) were used to interpret the Curie points. The most common magnetic minerals in igneous rocks and their respective Curie point temperatures include magnetite 575–585°C, hematite 680°C, and pyrrhotite 320°C. To characterize

the domain state of the magnetic minerals, we conducted isothermal remanent magnetization (IRM) acquisition experiments, which may be used to characterize the composition and the grain size of the ferromagnetic mineral(s) that are responsible for carrying the remanence and the stability of the magnetization (Butler, 1992; Dunlop, 1972, 1981; Dunlop et al., 1973). These experiments involve 17–20 magnetization steps to a peak field of 2.5 T. After a specimen reached saturation, an increasingly larger back-field was applied. The back-field was increased until net magnetic moment reached a remanence of zero; the applied field at which the magnetic moment was reduced to zero is the coercivity of the remanence. Back-field IRM (BIRM) typically involved 5–10 demagnetization steps up to 0.06 T. The shape of the IRM acquisition and the BIRM curves aided with identifying the grain composition (e.g., titanomagnetite, titanomaghemite, hematite), the magnetic grain size, and the domain state (single domain, pseudosingle domain, or multidomain) of the dominant magnetic mineral phase present (Dunlop, 1972, 1981; Dunlop et al., 1973).

Paleomagnetic methods

Samples were progressively demagnetized in an alternating field, and the remanent magnetization measured, typically in 10 to 25 steps to a maximum field of 120 mT using a ASC Scientific D-TECH 2000 AF-demagnetizer. Samples with high coercivity were treated with thermal demagnetization (TH) up to a maximum of 630°C, with most samples being fully demagnetized at 580°C. Thermal demagnetization experiments on replicate specimens, to compare with AF demagnetization behavior, were conducted with an ASC Scientific TD48 thermal demagnetizer. Principal component analysis (Kirschvink, 1980) was used to determine the best-fit line through selected demagnetization data points for each sample using Remasoft 3.0 (Chadima and Hrouda, 2006) (Fig. 4; Table 2). For most samples, a single best-fit line to the demagnetization data was obtained. Best-fit magnetization vectors involved 5 to 18 data points, but as few as 3 to as many as 25 were used,

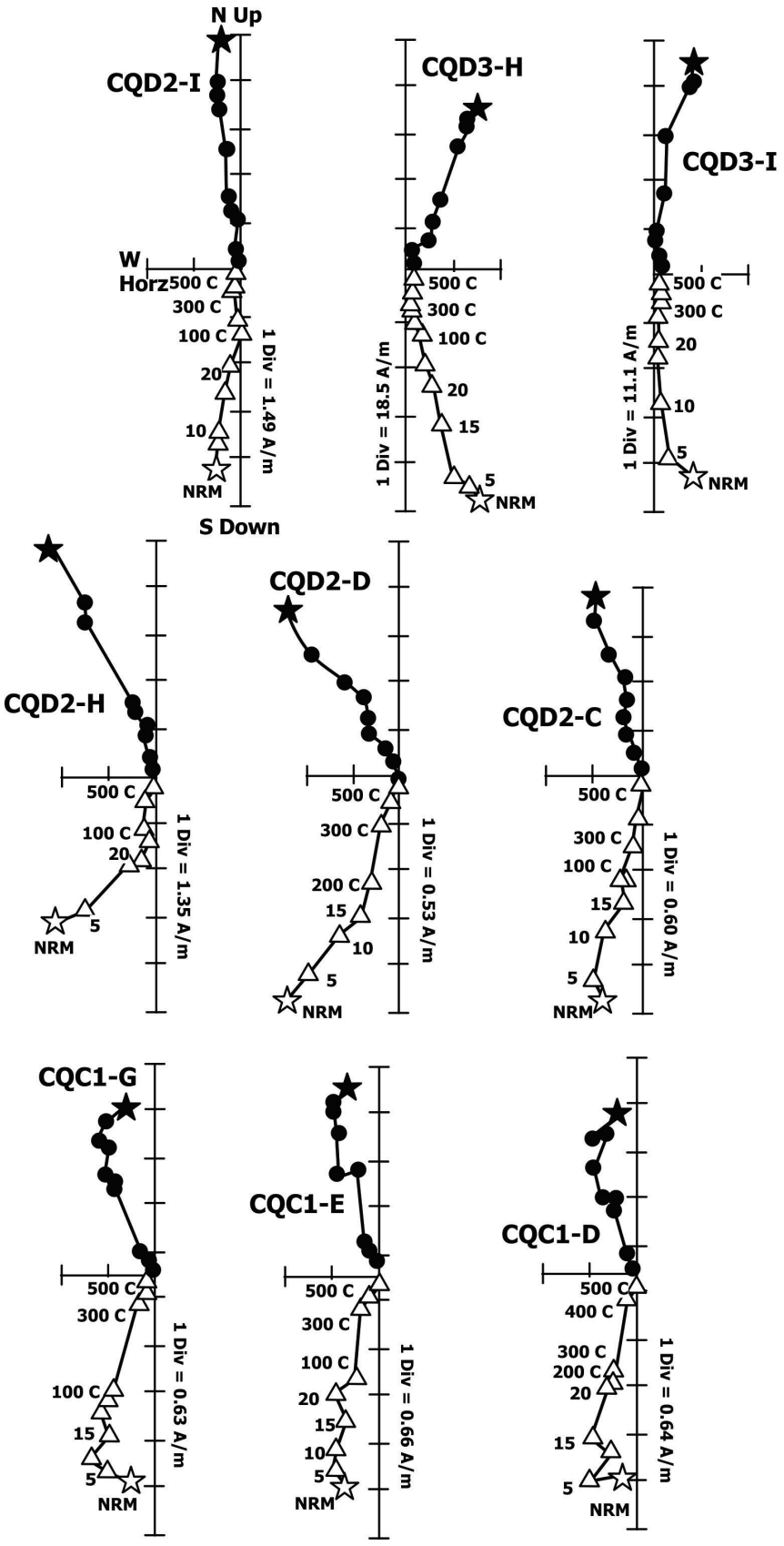

Figure 4. Orthogonal demagnetization diagrams (Zijderveld, 1967) showing alternating field and thermal demagnetization behavior of representative samples. Each sample was demagnetized from 5 to 20 mT in 5 mT steps, and from 100° to 500°C in 100°C steps. Declinations are plotted on the horizontal plane (circles) and inclinations are plotted on the vertical plane (triangles). Individual steps (mT, °C) are labeled on the vertical plane.

Table 2. Paleomagnetic data from the Rio del Oso dike swarm, Chili Quadrangle, Española Basin, NM.

SITE	N	No	R	α_{95}	*k*	Dec	Inc	VGB Lat	Long	UTM Northing	Easting
CQ1	7	7	6.95	5.7	111.9	359.1	45.3	80.4	79.2	390359	3995374
CQ2*	4	8	3.51	40.7	6.1	340.8	43.1	70.2	135.2	390376	3995418
CQ3	5	7	3.93	6.0	163.6	356.4	12.2	59.7	81.7	390383	3995457
CQ4D	8	8	7.97	3.6	241.4	342.2	50.3	74.1	149.5	390404	3995519
CQ5B	6	8	4.90	3.9	296.1	335.3	45.2	66.7	146.7	390403	3995612
CQ6B	7	8	6.32	8.7	49.1	335.8	21.1	56.1	121.9	390409	3995649
CQ7A	5	8	3.96	10.7	75.2	350.2	55.4	81.9	162.7	390393	3995622
CQ7B	8	8	7.94	5.4	107.8	336.1	44.4	67.1	143.8	390393	3995622
CQ7C	8	8	7.88	7.4	57.6	350.0	46.2	77.8	120.8	390393	3995622
CQB1	8	8	7.95	4.7	141.6	344.2	46.1	73.9	135.6	391097	3995238
CQB2	reject	-	-	-	-	-	-	-	-	391097	3995238
CQB3*	4	8	3.75	27.4	12.2	328.9	27.1	54.7	133.8	391097	3995238
CQB4	5	8	4.99	3.7	634.7	333.1	43.2	64.4	145.7	390853	3995859
CQB5*	5	8	4.43	31.2	7.0	357.4	-15.4	46.2	78.1	390856	3995857
CQB6	7	8	6.90	7.9	59.5	339.4	41.7	68.6	135.3	390858	3995856
CQB7	5	8	3.28	5.1	226.1	355.4	30.1	69.5	87.6	390859	3995855
CQB8	6	8	5.98	3.8	319.9	342.2	46.9	72.9	141.5	390860	3995854
CQB8_2	5	8	4.98	5.2	214.3	344.3	48.9	75.2	143.6	390861	3995853
CQB9	6	8	5.97	5.2	169.4	339.1	42.1	68.4	136.3	390862	3995852
CQB10	8	8	7.78	10.1	31.3	272.2	68.5	28.8	208.9	390864	3995854
CQB11	reject	-	-	-	-	-	-	-	-	390866	3995851
CQB14	8	8	7.90	6.6	71.7	332.3	46.2	64.7	151.6	390878	3995041
CQB15	5	8	3.98	6.7	191.7	332.1	14.7	51.8	122.5	390878	3995041
CQC1	5	8	4.97	6.5	138.6	339.1	47.8	71.0	148.0	390724	3995391
CQC2	6	8	5.96	6.4	112.1	348.7	48.1	78.4	129.6	390724	3995391
CQC3	7	8	3.92	14.8	39.7	339.9	47.9	71.8	146.7	390719	3995369
CQC5	5	6	4.97	7.1	118.3	345.1	54.2	77.7	160.9	390730	3995393
CQC6	6	7	5.94	7.6	78.0	344.9	45.9	74.6	133.6	390730	3995396
CQC7	7	7	6.94	6.2	97.0	345.2	49.8	76.4	145.1	390730	3995396
CQC8	5	6	4.90	12.3	39.9	013.2	45.8	75.7	18.7	388775	3995479
CQC9	4	6	3.96	11.1	69.9	006.8	45.1	78.8	40.8	388775	3995479
CQD1A*	5	8	4.64	24.0	11.1	319.6	62.7	58.4	191.0	388766	3995510
CQD1B#	7	8	6.74	12.8	23.2	058.2	-15.0	20.1	10.0	388766	3995510
CQD2A	7	8	6.98	3.5	295.6	333.8	62.1	68.9	191.5	390773	3995520
CQD2B	7	8	6.98	3.8	250.9	350.1	53.8	81.7	155.9	390773	3995520
CQD3B	8	8	3.99	5.5	280.2	351.9	70.1	71.3	239.0	390800	3995544
CQD4A	5	6	4.99	3.5	483.4	346.7	58.8	79.1	187.4	390820	3995582
CQD5A	5	6	4.98	5.3	209.8	332.2	61.2	67.6	187.8	390819	3995610
CQD5B	8	8	7.90	6.8	67.6	345.5	60.6	77.4	194.3	390819	3995610
CQD6A	4	6	3.97	8.8	111.2	337.1	53.4	71.0	162.9	390823	3995628
CQE1	reject	-	-	-	-	-	-	-	-	391105	3995242
CQE2	6	6	5.87	10.9	38.8	314.1	60.2	54.1	185.8	390804	3995588
CQE3	4	5	3.99	6.1	230.1	347.2	50.2	77.9	141.4	390813	3995597
CQE4	4	6	3.98	7.6	145.9	310.7	52.6	50.1	175.0	390806	3995600
CQE5	reject	-	-	-	-	-	-	-	-	388736	3995748
CQE6	3	5	2.97	15.5	64.7	338.3	26.6	60.6	120.8	388610	3995150
CQE7	4	5	3.98	7.5	151.6	347.1	52.1	78.7	149.6	390608	3995095
CQE8	reject	-	-	-	-	-	-	-	-	388613	3995094
CQE9	6	7	5.85	11.9	32.9	102.6	71.8	23.3	289.5	388602	3995058
CQE10	3	6	2.98	13.1	89.9	106.3	19.4	-7.0	326.1	388594	3995055
CQF1A	8	8	7.94	5.4	107.8	341.2	55.3	74.6	160.3	390711	3995335
CQF1C	4	6	3.93	10.8	41.3	322.6	40.8	55.8	152.6	390657	3995355
CQF2A	reject	-	-	-	-	-	-	-	-	388657	3995355
CQF2B*	4	6	3.82	23.1	16.8	305.8	60.6	48.1	188.4	388657	3995355
CQG1	reject	-	-	-	-	-	-	-	-	388593	3995033
CQG2	reject	-	-	-	-	-	-	-	-	388593	3995033
CQG3	reject	-	-	-	-	-	-	-	-	388593	3995033

EXPLANATION: Paleomagnetic data from the studied samples. Site is the sampling location; N is the number of samples used from the actual number of samples (No) collected at each site; R is the resultant vector length; α_{95} is the 95% confidence interval about the estimated mean direction, assuming a circular distribution; k is the best estimate of the Fisher precision parameter; Dec and Inc are the in situ declination and inclination; VGP Lat and Long are the latitude and longitude of the virtual geomagnetic pole for each site; UTM Northing and Easting are site coordinates (WGS84).
* in sampling location indicates site mean direction of high dispersion (α_{95} > 15°); # indicates site mean lies greater than 18° of the overall group mean direction.

and for less than 10% of the samples it was necessary to use the origin as an anchor. Magnetization vectors with maximum angular deviation values greater than 5 degrees were not included in site-mean calculations.

Petrography methods

Thin sections of samples from selected sites were prepared for petrographic analysis to identify the minerals present, characterize the sample textures, assess the relation of the magnetic minerals with the silicate minerals, and, if possible, assess the petrogenetic history of the magma from which the samples solidified. Hand samples were collected in the field, cut into billets, and sent to High Mesa Petrographics, Los Alamos, NM for preparation into thin sections. The thin sections were viewed using a Meiji ML 9000 polarizing microscope.

Results

Field observations and petrology

The western edge of the Española Basin is located about 10 km northwest of the city of Española, NM. The Española Basin is characterized by many rift-related geologic structures including faults of varying styles and motion, rift-basin sediment fill, basaltic intrusions, lava flows, and Quaternary terrace surfaces (Koning et al., 2005). Magmatism in the Espanola Basin is related to the Jemez Mountain volcanism and is also associated with rifting. Backbone-like dikes intruding the light-colored Ojo Caliente Sandstone of the Tesuque Formation (Santa Fe Group) are exposed throughout the study area. The studied dikes are tabular, fine grained, and mafic in composition (basalt). The dikes range from 0.5–3.5 m wide, form en echelon segments, and strike generally north-south. The minerals in the hand samples are 1.0–2.0 mm in length, often with elongated geometries, and include olivine (vitreous luster and olive-green color), plagioclase (white to gray tabular crystals), and minute augite (stubby prisms) phenocrysts. Many of the dikes have vesicles that may be filled with secondary calcite. At a few locations elongated vesicles and mineral lineations occur on the faces of the dikes.

Petrographic analyses

Petrographic analysis of the Rio del Oso dike samples from localities CQ1, 2, and 7 reveal hypocrystalline textures consisting of 50% glass and 50% crystals. The glassy component occurs as brown-colored isotropic material that is intergranular to the framework silicate minerals. Major minerals include olivine (10%), Ca-plagioclase (bytownite) (30%), augite (5%), and magnetite (<5%). The mineralogy was confirmed with powder x-ray diffraction analysis (Trujillo, 2014). Plagioclase ranges from 1.0 to 5.0 mm in length and occurs as euhedral phenocrysts and lath-like matrix crystals, many of which display swallowtail form. Olivine and clinopyroxene range from 1.0 to 2.0 mm in size and are subhedral to anhedral intergranular crystals. Magnetite is present as <0.10 mm, equant, disseminated grains, and as elongate grains with a dendritic habit. The presence of glass, as well as the swallowtail morphology of plagioclase laths and dendritic habit of the Fe-Ti oxide phases indicate undercooling of the host magma, consistent with shallow emplacement and rapid cooling (Lofgren 1983; Fig. 5). The mineralogy of the samples, along with their age and geographic location, supports their association with the Lobato Formation basalt flows. Thus, the mineral composition of the studied dikes is similar to that of Lobato basalt. Differences between individual flows and sampled intrusions include textural characteristics, including varying sizes of the phenocrysts, which can be attributed to the manner in which they cooled.

Paleomagnetic results

General demagnetization behavior

Fifty-seven sampling sites were established, with 48 sites yielding interpretable results. Additional samples from six of the sites are not used to calculate the group mean direction (Table 2). The nine uninterpretable sites did not yield stable end-point demagnetization behavior, and the six other sites yielded high dispersion between samples from the same site. We attribute these behaviors to either the rocks being struck by lightning, or chemically altered; samples from these fifteen sites are therefore excluded and our interpretation of the deformation in the region is based on forty-two sampling sites.

The majority of the samples were fully demagnetized with a combination of alternating field and thermal demagnetization treatments. Magnetization directions are well-grouped at the site level, with most sites yielding a single-component of magnetization that decays to the origin with less than ten percent of the NRM remaining after treatment in an alternating field of up to 20 mT and/or thermal treatment up to 525°C (Fig. 4). The majority of the samples contain a single characteristic remanent magnetization (ChRM), although some samples contain more than one magnetization component, which is randomized by about 300°C. We interpret these magnetizations as viscous remanent magnetization (VRM) overprints. After the VRM is removed, the remaining magnetization is likely a primary thermoremanent magnetization (TRM); which we interpret as the ChRM.

Paleomagnetic results from the forty-two sampling sites yield a group mean of D=344.0°, I=51.1°, α_{95}= 6.1°, k=14.1 (see Table 2 notes for an explanation of these parameters). The group-mean result is discordant to the <10 Ma pole direction of D=356.0°, I=54.4°, A_{95}=3.3° (Fig. 6; Table 3), with an inferred counterclockwise rotation of -12.0° ± 7.2, and a flattening of +13.3° ± 5.5° (Demarest, 1983; Beck, 1989).

To test the dispersion of the site-mean virtual geomagnetic poles (VGPs), we compared the average VGP dispersion to the predicated dispersion value for the latitude of the site (36.08° N) (Merrill and McElhinny, 1983). If secular variation has been adequately sampled, the observed angular dispersion estimate of site-mean VGPs should be consistent with the predicted value. The expected dispersion ranges from 13.5° to 17.7° (average = 15.6° ± 2.1°) (Table 2; Merrill and McElhinny, 1983; Cromwell et al., 2018). The estimated dispersion (S) of the forty-two site-mean

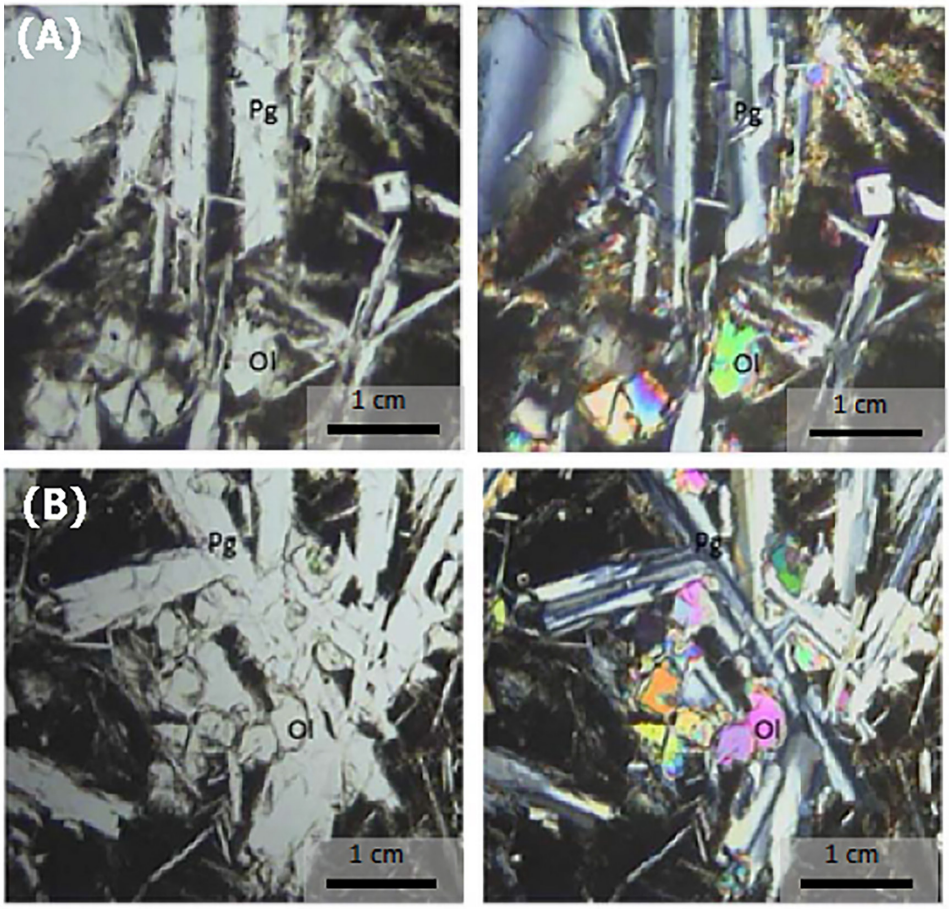

Figure 5. Representative photomicrographs of samples from the Rio del Oso dike swarm. The images on the left are in plane-polarized light and the images on the right are in cross-polarized light. (A) sample CQ3, (B) sample CQ4. The rocks display a hypocrystalline and olivine porphyritic texture. Minerals include olivine (Ol, high relief and high birefringence), plagioclase feldspar (Pg, lath shapes), and Fe-Ti oxide (elongate to dendritic shape, opaque). Interstitial glass is brown and isotropic.

directions yields a group-mean VGP dispersion of 24.4° ± 7.0° (95% confidence), a value that is statistically within the predicted VGP dispersion estimate. From this analysis, we suggest that paleomagnetic results from the forty-two sites may reflect either 1) a time interval covering a relatively long period of secular variation, or 2) tectonic deformation associated with rotation. As we discuss below, we prefer the latter interpretation of the data, given the field relationships.

Stability of the magnetization—contact test results

A contact test compares remanence directions in an igneous rock, the baked zone adjacent to the intrusion, and the unbaked zone away from the thermal aureole associated with the intrusion. An igneous intrusion heats the surrounding host rock and as both the magma and adjacent rock cool in Earth's magnetic field, the materials acquire a remanent magnetization that reflects the ambient field direction at the time of emplacement of the intrusion. The host rock often acquires a new remanence (i.e., remagnetization) in the same direction as the intrusion within a few centimeters to meters of the contact (Fig. 7). In general, if samples are taken from the intrusion and from the surrounding contact zone, and they yield the same magnetization direction, then the rocks from the intrusion are likely to carry a viable paleomagnetic direction (Everitt and Clegg, 1962; Calderone and Butler, 1984). Since the country rock and the igneous intrusion are generally very different rock types, agreement between the direction of magnetization of the intrusion and that of the baked region of the country rock provides strong evidence for the stability of the magnetization of the intrusion. The contact test compares remanence directions from the intrusion, the baked zone, and the unbaked zone (Fig. 7). In this study the host rock (Ojo Caliente Sandstone Member of Galusha and Blick, 1971), was sampled for a distance of 20 meters from the dike contact at intervals of about 1–2 m (Fig. 7), with a total of eight samples collected in the host rock, eight samples in the baked zone, and eight samples in the dike. The mean paleomagnetic direction from the host rock (sample CQB2) is D=225°, Inc=33°, the baked zone (CQB3) D=329°, I=30°, and the dike (CQB4) D=332°, I=44° (Fig. 7). Thus, paleomagnetic directions in sites located closer to the contact with the dike are similar to those of the intrusion, and we conclude that the results from the test are positive and that the remanence of the dike is a primary ChRM.

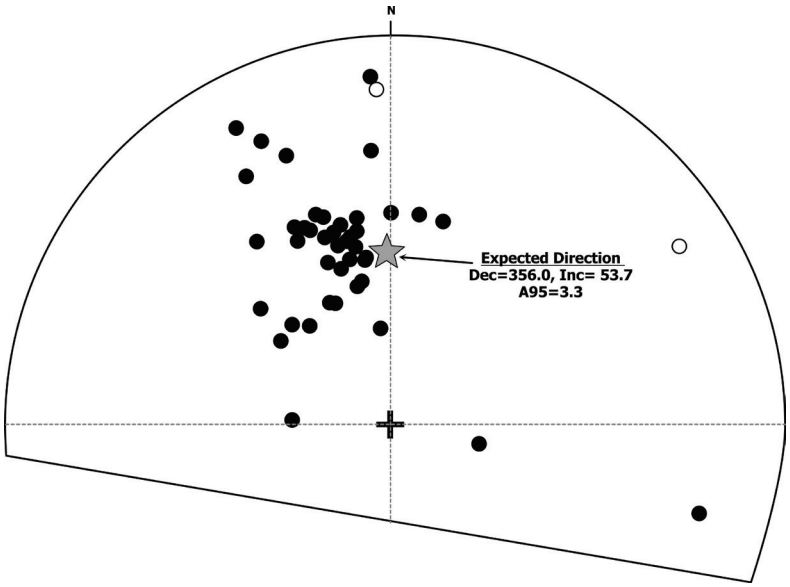

Figure 6. Paleomagnetic data from the sites that yielded interpretable results. Equal area lower hemisphere projection of all accepted site-mean directions. The excluded data were of high dispersion and are not shown. The open circles are reverse polarity sites. Gray star represents the <10 Ma field direction.

Table 3. Selected paleomagnetic poles for North America and corresponding expected directions.

					Expected Direction				
Age (Ma)	λ (N°)	Φ (E°)	A_{95}	K	Dec	Inc	A_{95}	Reference	Comments
0	90.0	180.0	-	-	360.0	55.5	-	a	GAD
15.9-11.6	88.3	209.0	6.3	N/A	358.3	56.7	5.1	b	Steens Mountain Basalts
15.9-11.6	88.7	171.6	4.0	N/A	358.4	55.7	3.3	b	Columbia River Basalts
***<10**	86.5	114.7	3.9	N/A	356.0	54.4	3.3	c	<10 Ma Poles
20	85.9	151.1	3.6	N/A	355.1	54.6	3.0	d	20 Ma mean pole
23	76.2	210.0	7.4	N/A	346.4	63.7	8.6	e	Colorado, Lake City Caldera[d]
0	86.5	180.7	3.0	96.2	355.8	56.5	2.4	f	20 Myr sliding window every 10 Myr
5	86.1	174.8	2.6	105.2	355.2	56.2	2.1	f	"
10	84.6	164.4	3.1	107.7	353.3	55.4	2.6	f	"
15	83.6	163.0	3.2	84.2	352.1	55.2	2.7	f	"
20	81.0	156.2	4.5	68.3	349.2	53.9	3.8	f	"
0	86.1	174.8	2.6	105.2	355.2	56.2	2.1	f	10 Myr sliding window every 5 Myr
10	85.0	168.1	2.0	94.2	353.8	55.8	1.6	f	"
20	83.3	164.2	2.7	75.6	351.7	55.3	2.2	f	"

EXPLANATION: Age (Ma) is the age range or age of the paleomagnetic pole; λ (N°) and Φ (E°) are latitude and longitude of the paleomagnetic reference pole; A_{95} is the semi-angle of the cone of 95% confidence about the pole; K is the best estimate of the precision parameter of the pole (Fisher, 1953) (N/A, not available); Expected Direction Dec & Inc are expected declination and inclination of the reference directions as calculated for the latitude and longitude of the Rio del Oso intrusions (36.08° N, 106.22° W); A_{95} is the estimated semi-angle of the cone of 95% confidence about the reference directions. Sources: a, pole and expected direction based on the hypothesis of a time-averaged geocentric axial dipole (GAD); b, Mankinen et al., 1987; c, Brown and Golombek (1985) mean of <10 Ma poles compiled by Irving and Irving (1982) (poles 1 through 12, with the exception of pole 5 from the Servilleta basalt flows north of the Española Basin and pole 9 from the Chamita Formation); d, Harrison and Lindh (1982), e, Colorado, Lake City Caldera; f, Besse and Courtillot (2002), synthetic North American poles.
*Our rotation estimates from the (CQ) Chili quadrangle basaltic dikes is based on the <10 Ma pole (highlighted red) calculated by Brown and Golombek (1985).

Rock magnetic experiment results

Rock magnetic experiments were conducted to determine the magnetic mineralogy and domain state of the principle magnetization carriers in the Lobato Formation intrusions. The results of the experiments indicate that the dominant magnetic mineral phase is a cubic Fe-Ti oxide of a restricted magnetic grain size, primarily pseudo-single domain titanomagnetite with a minor amount of coarse-grained maghemite or pyrrhotite.

Curie point estimates

Continuous susceptibility versus temperature results yield Curie-point estimates that range from ~100°C to 560°C. These temperatures are consistent with the presence of a range of moderate- to low-Ti composition magnetite with the presence of an iron sulfide phase (pyrrhotite) in some samples (Fig. 8). In sample CQ2 the heating and cooling curves vary widely, which indicates that there is a wide Curie-temperature decrease that is probably a result of the creation of new magnetite as a result of heating. Another possible explanation for the large variations between the heating and cooling curves is chemical alteration. These data provide evidence that the samples contain a magnetic phase that is capable of preserving a geologically stable magnetic phase that preserves a primary remanent magnetization.

IRM and BIRM experiment results

All Isothermal Remanent Magnetization (IRM) acquisition curves are steep

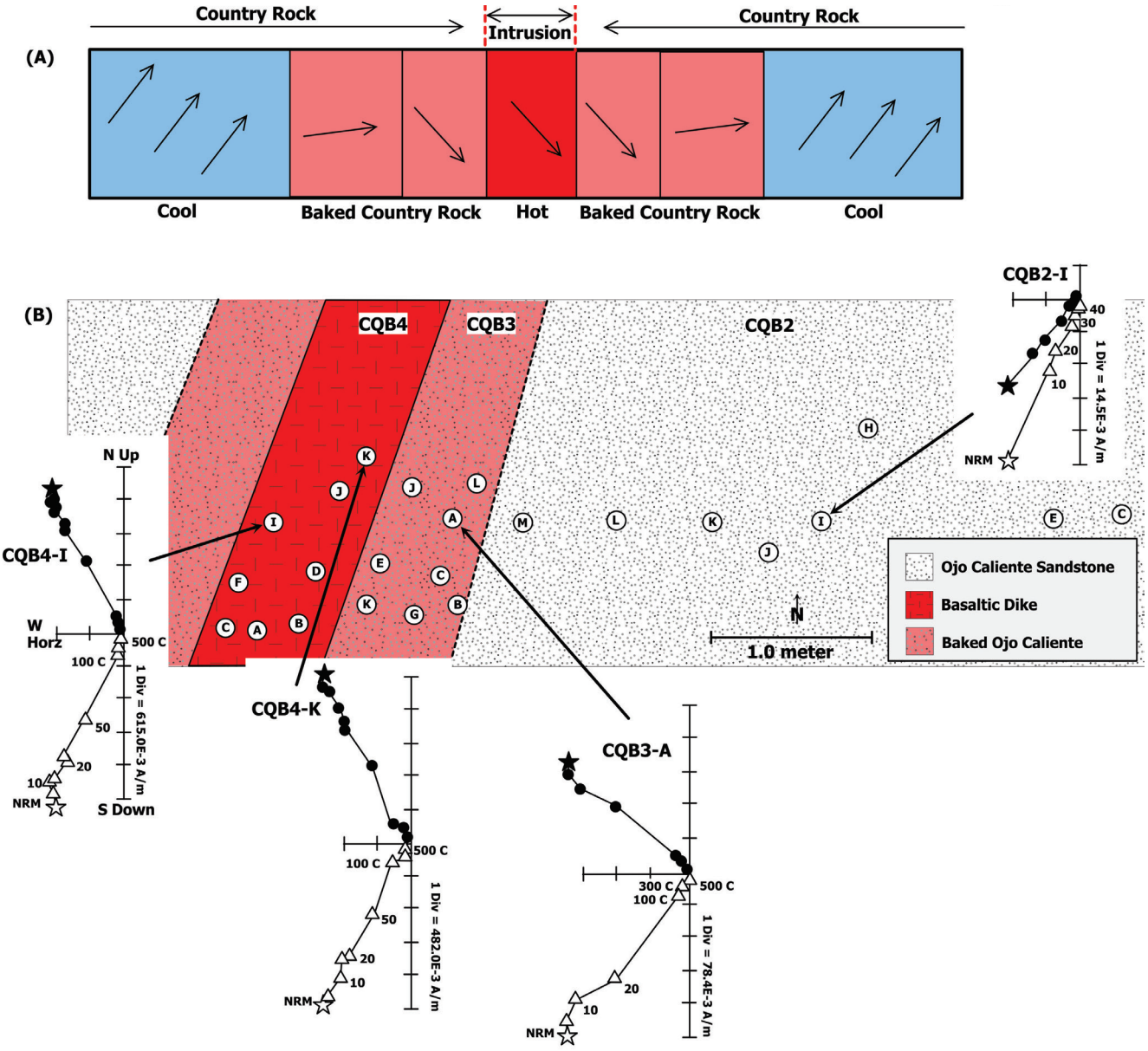

Figure 7. Contact test results. (A) Schematic diagram depicting a baked contact test that yields positive results. Emplacement of the intrusion (red) heats the country rock (blue), resulting in remagnetization. Near the intrusion the country rock yields a magnetization direction similar to that of the intrusion; farther from the intrusion the rocks are only partially reset. The arrows schematically represent differences in magnetic field direction. (B) Simplified illustration of one of the studied intrusions (CQB4) and its adjacent baked zone. The circled letters represent sample drill sites. The demagnetization diagrams show the behavior of selected samples during progressive alternating field and thermal demagnetization experiments.

and reach ~90% saturation by ~0.40 T, with the remaining 10% of the magnetization acquired up to 0.60 T (Fig. 9A). Backfield IRM curves yield coercivity of remanence values between 0.04–0.05 T, which is also consistent with a low Ti magnetite phase (Fig. 9B). The results indicate a dominance of magnetite, likely single domain titanomagnetite of a restricted grain size, along with the presence of titanomaghemite and likely pyrrhotite; we see no evidence of hematite (Özdemir and Dunlop, 1993). These data support the Curie point estimates in that the rocks contain a magnetic phase capable of preserving a stable remanence.

Discussion

Angular standard deviation of the virtual geomagnetic poles (VGPs)

Observed paleomagnetic declinations that are discordant, when inclinations are essentially identical to some expected value, can provide vertical axis rotation estimates for parts of the crust in either an absolute or a relative framework. Absolute rotation determinations require results that adequately sample the geomagnetic field over a sufficiently long time, which are then compared with a robust estimate of the time-averaged field based on independent paleomagnetic data (paleomagnetic poles) from the respective craton. Relative determinations, on the other hand, require sampling a single, laterally extensive datum (e.g., Wells and Hillhouse, 1989; Byrd et al., 1994; Sussman et al., 2006) located in several different structural settings (e.g., a regionally extensive ash-flow tuff). Under ideal circumstances, where either a time-averaged geomagnetic field is well-sampled, or a single datum consistently yields a very high-precision result, estimates of absolute vertical axis rotation typically have 95% confidence limits of ~4° to 10°, and relative vertical axis rotation estimates typically have confidence limits less than 5°. The paleomagnetic data from the Rio del Oso dike swarm allow for an estimate of absolute rotations relative to an adequately sampled geomagnetic field over a sufficiently long time, assuming they have adequately averaged secular variation of Earth's magnetic field.

As noted above, the expected dispersion of the VGPs for the latitude of north-central New Mexico during the mid to late Miocene ranges from 13.5° to 17.7° (average = 15.6° +/- 2.1°) (Table 2; Merrill and McElhinny, 1983; Cromwell et al., 2018). The angular standard deviation of magnetic poles obtained from the Rio del Oso dikes is 24.4° +/- 7.0° (95% confidence); a value which is statistically within the predicted VGP dispersion estimate, but greater than would be expected using paleosecular variation model G of McElhinny and McFadden (1997), which is based on VGP scatter during the past 5 Ma. Model G values are strictly valid only for VGPs derived from lava flows. Lava flows are erupted instantaneously relative to paleosecular variation and provide spot readings of the geomagnetic field at the time of eruption. Arguably, Model G dispersion estimates may not be appropriate when applied to slowly cooled intrusive rocks. Estimates of angular standard deviation

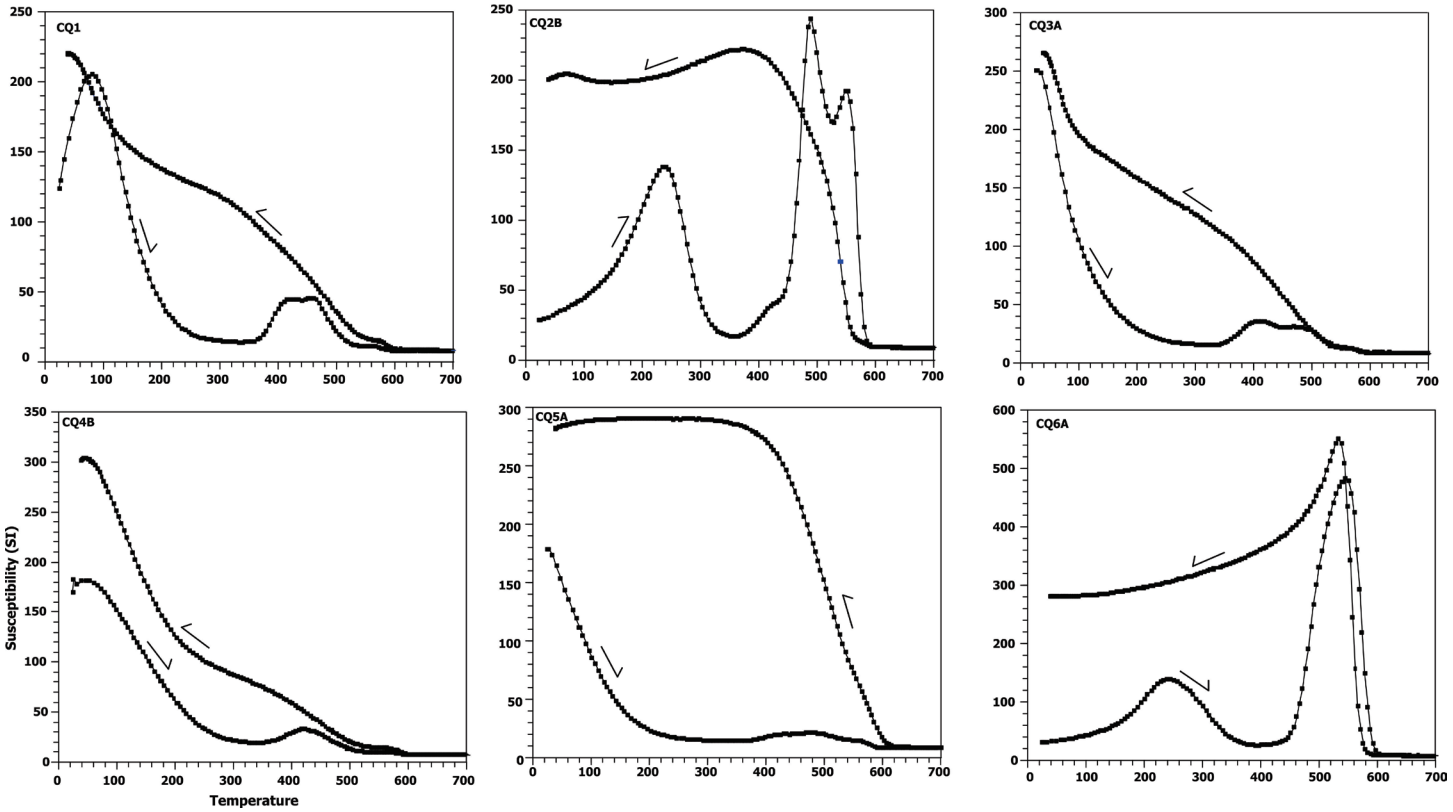

Figure 8. Continuous low-field susceptibility versus temperature experiments. Curie point estimates range from ~100 to 560 °C. These results indicate a range of moderate to low Ti- titanomagnetite compositions, and evidence of an Fe-sulfide phase (pyrrhotite).

from intrusive rocks are commonly less than predicted values, which probably results from some averaging of paleosecular variation at the site level during cooling and magnetization blocking (Frei et al., 1984; Harlan et al., 1994). However, using estimates of angular standard deviation alone to assess the viability of a data set from tectonically complicated areas should be viewed with caution. Complications such as faulting, inability to correct for unrecognized tilting, and other tectonic issues may lead to estimates of angular standard deviation that seem large, thus leading to erroneous inferences regarding the reliability or quality of the data.

In order to make an argument for tectonic deformation, a critical benchmark for a paleomagnetic data set is whether it has adequately averaged secular variation. A standard test is to compare observed dispersion of site-mean VGPs with the predicted dispersion (Merrill and McElhinny, 1983; Cromwell et al., 2018). If secular variation has been adequately sampled, the observed angular dispersion of site-mean VGPs should be consistent with that predicted for the paleolatitude of the sampling sites. If the observed dispersion of site-mean VGPs is less than predicted, a likely explanation is that the group mean represents a population of site mean directions that did not sample a time interval covering the periodicities of secular variation ($\leq 10^5$ yrs). The opposite situation is presented by a VGP dispersion that is substantially greater than predicted. In this case, it is probable that there is a source of VGP dispersion beyond secular variation. Often, a high dispersion can be explained by a tectonic disturbance within the sampling region, or there is difficulty in determining the site-mean ChRM directions. The latter is unlikely for our study of the Rio del Oso dike swarm because the demagnetization behavior is relatively straightforward (Fig. 4). We argue that the higher than predicted value likely represents a tectonic disturbance, although these conclusions should be viewed with a certain level of caution. For the interval from 5 Ma to 45 Ma, the amplitude of VGP dispersion in all latitude bands is greater than that for the 0 Ma to 5 Ma interval cited above. For example, in the band of latitude centered on 10° N, VGP dispersion is ~19° for 5 to 45 Ma and ~13° for 0 to 5 Ma. This may also be a factor to explain the higher than predicated value observed in our data set from the Rio de Oso dike swarm.

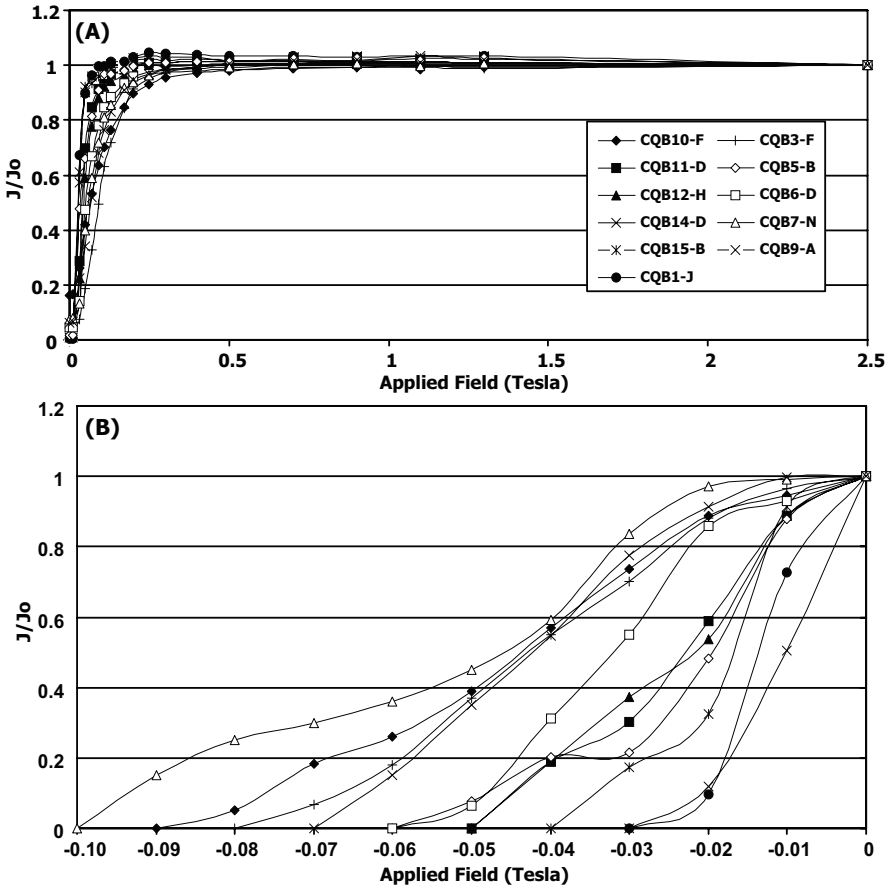

Figure 9. Isothermal remanent magnetization (IRM) and back-field IRM experiments. (A) Normalized isothermal remanent magnetization (IRM) from representative samples. The steep acquisition and saturation by ~0.4 T is indicative of titanomagnetite of a restricted single domain to pseudo-single-domain grain size. (B) Normalized back-field isothermal remanent magnetization acquisition demagnetization curves from representative samples. Coercivity of remanence values are typical of titanomagnetite with a low-Ti composition.

Vertical axis rotation in the Rio Grande Rift

Rocks located at or near the surface of the Earth generally behave in a brittle manner when deformed under moderate strain rates. The Earth's crust deforms by distortion, displacement, and rigid-body rotation. In the case of rigid-body rotations, vertical axis rotations are often difficult to identify based on macro- and micro-structural analysis. The application of paleomagnetism, however, has proven to be a reliable technique for quantifying vertical axis rotation directions and magnitudes. Many paleomagnetic studies have been conducted to identify vertical axis rotations, or lack thereof, associated with regional and localized faulting (e.g., Gillett and Van Alstine, 1982; Ron et al., 1984; Hudson and Geissman, 1987, 1991; Janecke et al., 1991; Hudson, 1992; Cashman and Fontaine, 2000; Hudson et al., 1994; Wawrzyniec et al., 2002; Petronis et al., 2002, 2007). Several workers have conducted studies in the Española Basin and have implemented the use of paleomagnetic analysis to assess whether or not vertical axis rotation has in fact taken place within the region (Brown and Golombek 1985, 1986; Salyards et al., 1994; Hudson et al., 2004). The Española Basin block is bounded by a series of accommodation structures. These include the Tijeras-Cañoncito fault zone to the south, the Pajarito fault zone to the west, and the Embudo fault zone to the north (Kelley, 1977; Muehlberger, 1979; Brown and Golombek, 1986). A

kinematic model of block rotation in the Española Basin was developed by Muehlberger (1979), advanced by Brown and Golombek (1986), and further supported by Harlan and Geissman (2009). The model was in part developed based on the results from several paleomagnetic data sets from across the Española Basin, all of which yield internally as well as spatially consistent results. Previous data sets indicate that vertical axis rotation amounts vary significantly from the western margin of the basin to the eastern margin of the basin. A compilation of all the data along the western margin of the Española Basin indicates that the block rotation direction is dominantly counterclockwise with a domain near the western basin margin showing a component of clockwise rotation (Fig. 10A). This observation arguably reflects heterogeneous strain accommodation across the basin. This further suggests that movement along the western margin has been greater than it is on the eastern margin of the Española Basin (Salyards et al., 1994). Alternatively, Sussman et al. (2011) conducted a study of the Bandelier Tuff within the Española Basin block to assess possible components of vertical axis rotation within the basin. The results of the study were interpreted to indicate that no vertical axis rotations occurred during Quaternary time. It was concluded by Sussman et al. (2011) that vertical axis rotation along the western Española Basin block was not associated with regional deformation, but rather attributed to localized deformation events.

Vertical axis rotation in the Española Basin

The group mean result from forty-two paleomagnetic sites established in the Rio del Oso dike swarm record a modest, yet statistically significant component of counter-clockwise rotation relative to the average <10 Ma pole direction, with an inferred rotation of -12.0° ± 7.2° and flattening of +13.3° ± 5.5°. As noted above, this is an absolute rotation estimate relative to the selected <10 Ma pole (Table 3). The sampling sites are distributed over a 4.8 km^2 area and it is probable that the group mean direction may not be representative of along-strike and spatially variable vertical axis rotations across the area. Based on the dispersion of the paleomagnetic data, some sites record greater or less than the amount of vertical axis rotation based on the collective group mean direction. Numerous small-scale synthetic and antithetic faults crosscut the sampling area and may have facilitated differential vertical-axis rotation in the area.

Estimates from previous studies (Brown and Golombek 1985, 1986; Salyards et al., 1994; Hudson et al., 2004) indicate tectonic rotation values and directions similar to those reported here. In addition, other geologic data (Kelley 1977, 1979) suggest that block rotations are likely taking place. Paleomagnetic results from this study indicate that the western margin of the Española Basin has experienced a modest magnitude -12.0° ± 7.2° counter-clockwise rotation about the vertical axis. The rotation is ascribed to post-middle Miocene regional extension. The model proposed by many workers to explain counter-clockwise vertical axis rotations is depicted in Figure 10B. Within the Española Basin, and more locally within the Chili Quadrangle, a complex array of faults are thought to transfer components of both dip-slip and strike-slip deformation across the region. There are two major faults in the region: the Cañada del Amagre and the Santa Clara fault systems. Movement along these structures and other minor faults associated with continental extension has likely facilitated rotation in this part of the Española Basin.

Conclusions

The paleomagnetic data presented here provide evidence for a modest amount of counter-clockwise vertical-axis rotation along the western margin of the Española Basin. The rotation is likely associated with extension within the Rio Grande rift. The supporting rock-magnetic experiments and field tests indicate that the magnetization data are geologically stable and thus represent

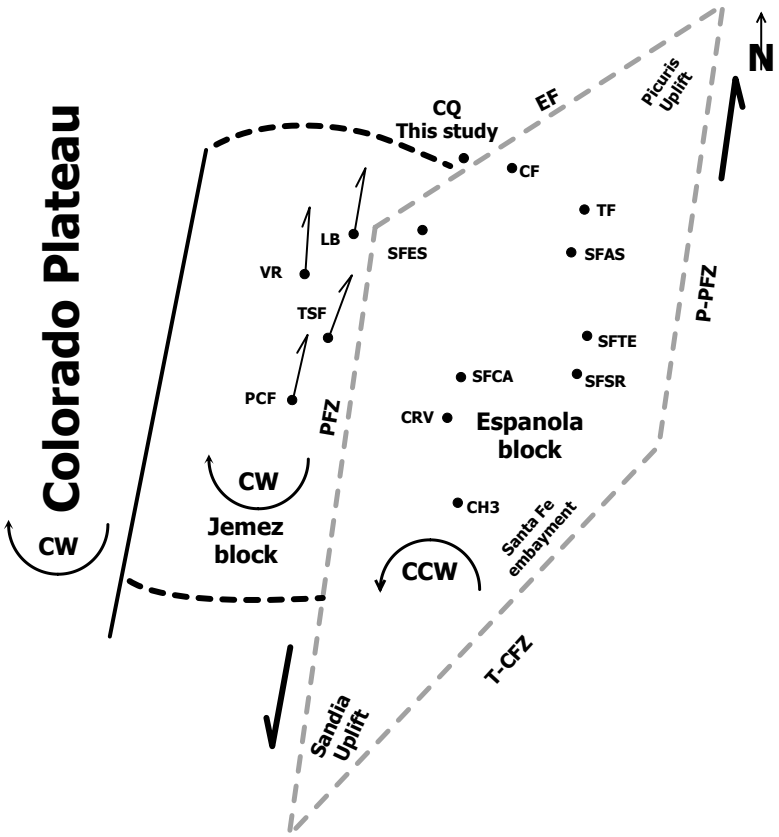

Figure 10A. Schematic model proposed by Brown and Golombek (1986) of the apparent rotations within the Jemez block and other site locations in the Española block (cf. Fig. 1). Deviation from geographic north in the Jemez block indicates an apparent vertical axis rotation; the lines deflected to the right indicate a clockwise (CW) rotation. Labels explained in Figure 10B caption.

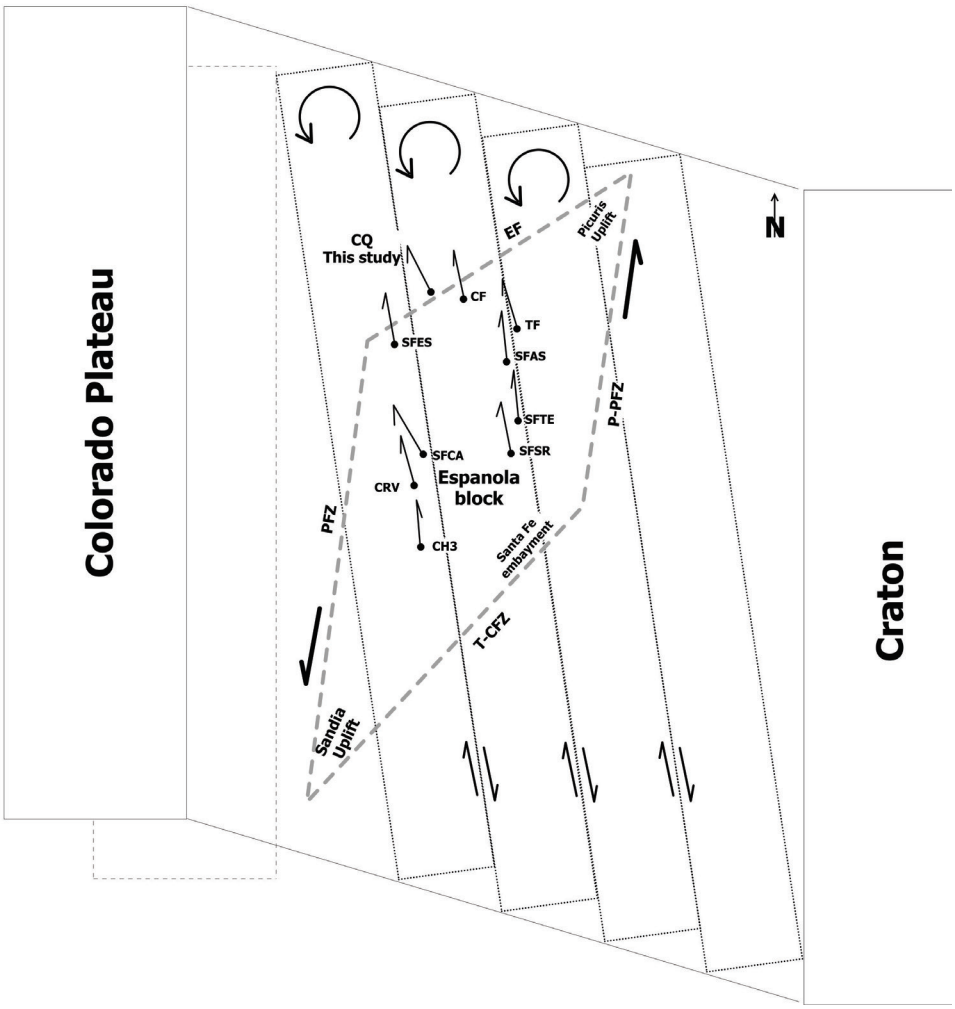

Figure 10B. Simplified model of inferred block rotations in the Española basin of the Rio Grande rift, based in part on paleomagnetic data from Muehlberger (1979), Barghoorn (1981), Brown and Golombek (1986), and Harlan and Geissman (2009). Deviation of the arrows from geographic north indicate apparent magnitude of rotation; thus lines to the left of north indicate counter-clockwise (CCW) rotation. The block model on which the inferred paleomagnetic rotations are shown is after Wawrzyniec et al. (2002) and schematically depicts how crustal blocks or sets of blocks may have rotated in a CCW sense during Neogene dextral transtension. The data from the Oso de Arroyo dike swarm are rotated counter-clockwise and are situated north of the concealed trace of the Embudo fault. This extends the domain(s) of counter-clockwise rotation to the north. Abbreviations: Sedimentary rock units—CF, Chamita Formation; TF, Tesuque Formation; SFTE, Tesuque Formation, Nambé Member; SFAS, Tesuque Formation, Skull Ridge Member; SFSR, Tesuque Formation, Nambé Member; SFES and SFCA, Chamita Formation. Igneous rock units—CRV, Cerros del Rio volcanics; CH3, Cerrillos Hills and Ortiz Mountains; CQ, Chili Quadrangle Lobato intrusions (this study); LB, Lobato basalt; PCF, Paliza Canyon Formation; TSF, Tschicoma Formation; VR, Valles rhyolite. Major faults—T-CFZ, Tijeras-Cañoncito fault zone; PFZ, Pajarito fault zone; EF, Embudo fault zone; P-PFZ, Picuris-Pecos fault zone.

primary TRMs. Petrology demonstrates that the dikes are similar along strike and represent the same magma source emplaced into the shallow crust during extension. Together these data provide insight regarding the tectonic evolution of the western margin of the Española Basin. Paleomagnetic data from rocks of various ages and types throughout the Española Basin yield consistent results indicating that counter-clockwise rotation accompanied Neogene to recent extension within the Rio Grande rift. Problems exist with the regional coverage of paleomagnetic data and with the averaging out of paleosecular variation. It is apparent, however, that the consistency between different studies supports counter-clockwise block rotation across this latitude of the rift. The Rio Grande rift continues to extend at a slow rate and these data strongly suggest that the rift continues to evolve. The western margin of the Española Basin has been influenced by greater rotations than the eastern margin of the basin, which suggests that the faults within the rift heavily influence the degree of rotation between the blocks. The interaction of the faults located within the rift are responsible for the intra-rift rotations that continue today.

Acknowledgements

This paper represents a major component of Rhonda Trujillo's Masters Thesis research. This work was funded by grants-in-aid of research to Rhonda Trujillo from the New Mexico Geological Society, the Four Corners Geological Society, and the New Mexico Highlands University Sigma Xi Chapter. Powder x-ray diffractometry analysis was supported by National Science Foundation Grant DMR-1523611 (PREM) awarded to Dr. Tatiana Timofeeva. A special thanks to Dr. Linda LaGrange for her support of faculty and student research at New Mexico Highlands University. All data related to this project will be made available at http://www.nmhugeology.com/, the paleomagnetic data will be uploaded to the MagIC database (https://www2.earthref.org/MagIC), FAIR principles, and all data sets may be requested from the mspetro@nmhu.edu. Datasets for this research are also included in this paper. A very special thank you to Adam Brister, Dani Cedillo, Marine Foucher, Darren Lemen, Andrew Romero, Salvador Sena, and Nathan Wales for field and laboratory assistance. We also thank the reviewers Dr. Laurie Brown and Dr. Bruce Allen for constructive reviews.

References

Aldrich, M.J., Jr., 1986, Tectonics of the Jemez Lineament in the Jemez Mountains and Rio Grande rift: Journal of Geophysical Research, v. 91, p. 1753–1762.

Aldrich, M.J., Jr., and Dethier, D.D., 1990, Stratigraphic and tectonic evolution of the northern Española Basin, Rio Grande rift, New Mexico: Geological Society of America Bulletin, v. 102, p. 1695–1705.

Anderson, E.M., 1951, The Dynamics of Faulting and Dyke Formation with Applications to Britain: Edinburgh, Oliver and Boyd, 206 p.

Atwater, T., and Stock, J., 1998, Pacific-North American plate tectonics of the Neogene southwestern United States: an update, *in* Ernst, W.C., and Nelson, C.A., eds., Integrated Earth and Environmental Evolution of the Southwestern United States: Columbia, MD, Bellwether Publishing, p. 393-420.

Bachman, G.O., and Mehnert, H.H., 1978, New K-Ar dates and the late Pliocene to Holocene geomorphic history of the central Rio Grande region, New Mexico: Geological Society of America Bulletin, v. 89, p. 283–292.

Baer, G., 1991, Mechanisms of dike propagation in layered rocks and in massive, porous sedimentary rocks: Journal of Geophysical Research, v. 96, p. 11911–11929.

Baldridge, W.S., Damon, P.E., Shafiqullah, M., and Bridwell, R.J., 1980, Evolution of the central Rio Grande rift, New Mexico: new potassium-argon ages: Earth and Planetary Science Letters, v. 51, p. 309–321.

Baldridge, W.S., Perry, F.V., Vaniman, D.T., Nealey, L.D., Leavy, B.D., Laughlin, A.W., Kyle, P., Bartov, Y., Steinitz, G., and Gladney, E.S., 1991, Middle to late Cenozoic magmatism of the southeastern Colorado Plateau and central Rio Grande Rift (New Mexico and Arizona, U.S.A.): a model for continental rifting: Tectonophysics, v. 197, p. 327–354.

Barghoorn, S., 1981, Magnetic-polarity stratigraphy of the Miocene type Tesuque Formation, Santa Fe Group, in the Espanola valley, New Mexico: Geological Society of America Bulletin, v. 92, p. 1027–1041.

Beck, M., 1989, Paleomagnetism of continental North America: implications for displacement of crustal blocks within the Western Cordillera, Baja California to British Columbia, *in* Pakiser, L., and Mooney, W., eds., Geophysical Framework of Continental United States: Geological Society of America, Memoir 172, p. 471–492.

Besse, J., and Courtillot, V., 2002, Apparent and true polar wander and the geometry of the geomagnetic field over the last 200 Myr: Journal of Geophysical Research, v. 108 (B11), 2300, doi: 10.1029/2000JB000050.

Brown, L.L., and Golombek, M.P., 1985, Tectonic rotations within the Rio Grande rift: evidence from paleomagnetic studies: Journal of Geophysical Research, v. 90, p. 790–802.

Brown, L.L., and Golombek, M.P., 1986, Block rotations in the Rio Grande rift, New Mexico: Tectonics, v. 5, p. 423–438.

Butler, R.F., 1992, Paleomagnetism: magnetic domains to geologic terranes: Boston, Blackwell Scientific, 238 p.

Byrd, J.O.D., Smith, R.B., and Geissman, J.W., 1994, The Teton fault, Wyoming: topographic signature, neotectonics, and mechanisms of deformation: Journal of Geophysical Research, v. 99, p. 20095–20122.

Calderone, G., and Butler, R.F., 1984, Paleomagnetism of Miocene volcanic rocks from southwestern Arizona: tectonic implications: Geology, v. 12 p. 627–630.

Cashman, P.H., and Fontaine, S.A., 2000, Strain partitioning in the northern Walker Lane, western Nevada and northeastern California: Tectonophysics, v. 326, p. 111–130.

Chadima, M., and Hrouda, F., 2006, Remasoft 3.0: a user-friendly paleomagnetic data browser and analyzer: Travaux Geophysiques, v. XXVII, p. 20–21.

Chapin, C.E., 1988, Axial basins of the northern and central Rio Grande rift, *in* Sloss, L.L., ed., Sedimentary Cover—North American Craton: Geological Society of America, Decade of North American Geology, v. D-2, p. 165–170.

Chapin, C.E., and Cather, S.M., 1994, Tectonic setting of the axial basins of the northern and central Rio Grande rift, *in* Keller G.R., and Cather, S.M., eds., Basins of the Rio Grande Rift: Structure, Stratigraphy, and Tectonic Setting: Geological Society of America, Special Paper 291, p. 5–25.

Cox, A., and Doell, R.R., 1960, Review of paleomagnetism: Geological Society of America Bulletin, v. 71, p. 645–768.

Cromwell, G., Johnson, C.L., Tauxe, L., Constable, C.G., and Jarboe, N.A., 2018, PSV10: a global data set for 0–10 Ma time-averaged field and paleosecular variation studies: Geochemistry, Geophysics, Geosystems, v. 19, 1533–1558.

Dalrymple, G.B., and Hirooka, K., 1965, Variation of potassium, argon, and calculated age in a late Cenozoic basalt: Journal of Geophysical Research, v. 70, p. 5291–5296.

Demarest, H.H., 1983, Error analysis for the determination of tectonic rotations from paleomagnetic data: Journal of Geophysical Research, v. 88, p. 4321–4328.

Dethier, D., and Manley, K., 1985, Geologic map of the Chili Quadrangle, Rio Arriba County, New Mexico: U.S. Geological Survey, Miscellaneous Field Studies Map MF-1814, scale 1:24,000.

Dethier, D.P., Aldrich, M.J., Jr., and Shafiqullah, M., 1986, New K-Ar ages for Miocene volcanic rocks from the northeastern Jemez Mountains and Tejana Mesa, New Mexico: Isochron West, no. 47, p. 1–14.

Dunlop, D.J., 1972, Magnetic mineralogy of unheated and heated red sediments by coercivity spectrum analysis: Geophysical Journal International, v. 27, p. 37–55.

Dunlop, D.J., 1981, Paleomagnetic evidence for Proterozoic continental development: Philosophical Transactions of the Royal Society, v. 301, p. 265–277.

Dunlop, D.J., Hanes, J.A., and Buchan, K.L., 1973, Indices of multidomain magnetic behavior in basic igneous rocks: alternating field demagnetization, hysteresis, and oxipetrology: Journal of Geophysical Research, v. 78, p. 1387–1394.

Everitt, C.W.F., and Clegg, J.A., 1962, A field test of paleomagnetic stability: Geophysical Journal of London, v. 6, p. 312–319.

Fisher, R.A., 1953, Dispersion on a sphere: Proceedings of the Royal Society of London, Series A, v. 217, p. 295–305.

Frei, L.S., Magill, J., and Cox, A., 1984, Paleomagnetic results from the central Sierra Nevada: constraints on reconstruction of the western United States: Tectonics, v. 3, p. 157–177.

Galusha, T., and Blick, J.C., 1971, Stratigraphy of the Santa Fe Group, New Mexico: American Museum of Natural History Bulletin, v. 144, p. 7–127.

Gardner, J.N., Goff, F., Garcia, S., and Hagen, R.C., 1986, Stratigraphic relations and lithologic variations in the Jemez volcanic field, New Mexico: Journal of Geophysical Research, v. 91, p. 1763–1778.

Gillett, S.L., and Van Alstine, D.R., 1982, Remagnetization and tectonic rotation of the upper Precambrian and lower Paleozoic strata from the Desert Range, southern Nevada: Journal of Geophysical Research, v. 87, p. 10929–10953.

Golombek, M.P., McGill, G.E., and Brown, L.L., 1983, Tectonic and geologic evolution of the Española Basin, Rio Grande rift: structure, rate of extension, and relation to the state of stress in the western United States: Tectonophysics, v. 19, p. 483–507.

Grauch, V.J.S., and Bankey, V., 2003, Aeromagnetic interpretations for understanding the hydrogeologic framework of the southern Española Basin, New Mexico: U.S. Geological Survey, Open-File Report 03-124, p. 2–39.

Grauch, V.J.S., Bauer, P.W., Drenth, B.J., and Kelson, K.I., 2017, A shifting rift—geophysical insights into the evolution of Rio Grande rift margins and the Embudo transfer zone near Taos, New Mexico: Geosphere, v. 13, p. 870–910.

Harlan, S.S., and Geissman, J.W., 2009, Paleomagnetism of Tertiary intrusive and volcaniclastic rocks of the Cerrillos Hills and surrounding region, Española Basin, New Mexico, U.S.A.: assessment and implications of vertical-axis rotations associated with extension of the Rio Grande rift: Lithosphere, v. 1, p. 155–173.

Harlan, S.S., Snee, L.W., and Brearley, A.J., 1994, Paleomagnetism of the middle Proterozoic Laramie anorthosite complex and Sherman Granite, southern Laramie Range, Wyoming and Colorado: Journal of Geophysical Research, v. 99, p. 17997–18020.

Harrison, C.G.A., and Lindh, T., 1982, A polar wandering curve for North America during the Mesozoic and Cenozoic, Journal of Geophysical Research, v. 87, p. 1903–1920.

Hopkinson J., 1889, Magnetic and other physical properties of iron at a high temperature: Philosophical Transactions of the Royal Society of London A, v. 180, p. 443–465.

Hudson, M.R., 1992, Paleomagnetic data bearing on the origin of arcuate structures in the French Peak-Massachusetts Mountain area of southern Nevada: Geological Society of America Bulletin, v.104, p. 581–594.

Hudson, M.R., and Geissman, J.W., 1987, Paleomagnetic and structural evidence for middle Tertiary counterclockwise rotation in the Dixie Valley region, west-central Nevada: Geology, v. 15, p. 638–642.

Hudson, M.R., and Geissman, J.W., 1991, Paleomagnetic evidence for the age and extent of middle Tertiary counterclockwise rotation, Dixie Valley region, west-central Nevada: Journal of Geophysical Research, v. 96, p. 3979–4006.

Hudson, M.R., Sawyer, D.A., and Warren, R.G., 1994, Paleomagnetism and rotation constraints for the middle Miocene southwestern Nevada volcanic field: Tectonics, v. 13, p. 258–277.

Hudson, M.R., Thompson, R.A., Minor, S.A., and Warren, R.G., 2004, Counterclockwise declination anomaly in paleomagnetism of the Pliocene Cerros del Rio volcanic field, New Mexico: an expression of late Rio Grande rift distributed shear: Geologic Society of America, Abstracts with Programs, v. 36, no. 5, p., 436.

Irving, E., and Irving, G.A., 1982, Apparent polar wander paths Carboniferous through Cenozoic and the assembly of Gondwana: Geophysical Surveys, v. 5, p. 141–188.

Janecke, S.U., Geissman, J.W. and Bruhn, R.L., 1991, Correction to "Localized rotation during Paleogene extension in east central Idaho: paleomagnetic and geologic evidence" by Susanne U. Janecke et al.: Tectonics, v. 10, p. 657.

Kelley, V.C., 1977, Geology of the Albuquerque Basin, New Mexico: New Mexico Bureau of Mines and Mineral Resources, Memoir 33, 59 p.

Kelley, V.C., 1979, Tectonics, middle Rio Grande rift, New Mexico, *in* Riecker, R.D., ed., Rio Grande Rift, Tectonics and Magmatism: Washington, D.C., American Geophysical Union, p. 57–70.

Kelley, V.C., 1982, The right-relayed Rio Grande rift, Taos to Hatch, New Mexico: New Mexico Geological Society, Guidebook 33, p. 147–151.

Kirschvink, J.L., 1980, The least-squares line and plane analysis of paleomagnetic data: Geophysical Journal of the Royal Astronomical Society, v. 62, p. 699–718.

Koning, D., Skotnicki, S., Kelley, S., and Moore, J., 2005, Geologic Map of the Chili Quadrangle, Rio Arriba County, New Mexico: New Mexico Bureau of Geology and Mineral Resources, Open-File Geologic Map OF-GM 103, Scale 1:24,000.

Koning, D.J., Connell, S.D., Slate, J.L., and Wan, E., 2007, Stratigraphic constraints for Miocene-age vertical motion along the Santa Clara fault, Española Basin, north-central New Mexico: New Mexico Geological Society, Guidebook 58, p. 225–238.

Lofgren, G.E., 1982, Experimental studies on the dynamic crystallization of silicate melts, *in* Hargraves, R.B., ed., Physics of Magmatic Processes: Princeton University Press, p. 487–551.

Luedke, R., and Smith, R., 1978, Map showing distribution, composition and age of late Cenozoic volcanic centers in Arizona and New Mexico: U. S. Geological Survey, Miscellaneous Investigations Map I-1091-A.

MacFadden, B.J., 1977, Magnetic polarity stratigraphy of the Chamita Formation stratotype (Mio-Pliocene) of north-central New Mexico: American Journal of Science, v. 277, p. 769–800.

Mankinen, E.A., Larson, E.E., Gromme, C.S., Prevot, M., and Coe, R.S., 1987, The Steens Mountain (Oregon) geomagnetic polarity transition: Journal of Geophysical Research, v. 92, p. 8057–8076.

Manley, K., and Mehnert, H., 1981, New K-Ar ages of Miocene and Pliocene volcanic rocks in the northwestern Española Basin and their relationships to the history of the Rio Grande Rift: Isochron West, v. 30, p. 5-8.

McElhinny, M.W., and McFadden, P.L., 1997, Palaeosecular variation over the past 5 Myr based on a new generalized database: Geophysical Journal International, v. 131, p. 240–252.

Merrill, R.T., and McElhinny, M.W., 1983, The Earth's Magnetic Field: Its History, Origin, and Planetary Perspective: New York and London, Academic Press, 401 p.

Morgan, J.W., Sato, M., Matsuo, S. and King, C.-Y., 1986, Ultramafic xenoliths; clues to Earth's late accretionary history: Journal of Geophysical Research, Solid Earth, v. 91, p. 12375–12387.

Moscowitz, B.M., 1981, Methods for estimating Curie temperatures of titanomagnetites from experimental Js-T data: Earth and Planetary Science Letters, v. 53, p. 84–88.

Muehlberger, W.R., 1979, The Embudo fault between Pilar and Arroyo Hondo, New Mexico: an active intracontinental transform fault: New Mexico Geological Society, Guidebook 30, p. 77–82.

NMBGMR, 2003, Geologic map of New Mexico: Socorro, NM Bureau of Geology and Mineral Resources, scale 1:500,000.

Otofuji, Y., Matsuda, T., and Nohda, S., 1985, Opening mode of the Japan Sea inferred from the palaeomagnetism of the Japan Arc: Nature, v. 317, p. 603–604.

Özdemir, Ö, Dunlop, D.J., Moskowitz, B.M., 1993, The effect of oxidation on the Verwey transition in magnetite, Geophysical Research Letters, v. 20, I. 16, p. 1671–1674

Petronis, M.S., and Lindline, J., 2011, Paleomagnetic and geochemical data from the late Miocene Lobato Formation adjacent to the Santa Clara fault system, Chili quadrangle, Rio Arriba county, New Mexico: New Mexico Geology, v. 33, p. 27–39.

Petronis, M.S., Geissman, J.W., Oldow, J.S., and McIntosh, W.C., 2002, Paleomagnetic and $^{40}Ar/^{39}Ar$ geochronologic data bearing on the structural evolution of the Silver Peak extensional complex, west-central Nevada: Geological Society of America Bulletin, v. 114, p. 1108–1130.

Petronis, M.S., Geissman, J.W., Oldow, J.S., and McIntosh, W.C., 2007, Tectonism of the southern Silver Peak Range: paleomagnetic and geochronologic data bearing on the Neogene development of a regional extensional complex, central Walker Lane, Nevada: Geological Society of America, Special Paper 434, p. 81–106.

Prodehl, C., and Lipman, P.W., 1989, Crustal structure of the Rocky Mountain region, *in* Pakiser, L.C., and Mooney, W.D., eds., Geophysical Framework of the Continental United States: Geological Society of America, Memoir 172 , p. 249–284.

Ron, H., Freund, R., Garfunkel, Z., and Nur, A., 1984, Block rotation by strike slip faulting: structural and paleomagnetic evidence: Journal of Geophysical Research, v. 89, p. 6256-6270.

Salyards, S.L, Ni, J.F., and Aldrich, M.J., Jr., 1994, Variation in paleomagnetic rotations and kinematics of the north-central Rio Grande rift, New Mexico: Geological Society of America, Special Paper 291, p. 59–71.

Seager, W., and Morgan, P., 1979, Rio Grande rift in southern New Mexico, West Texas, and northern Chihuahua, *in* Riecker, R.D., ed., : Rio Grande Rift, Tectonics and Magmatism: Washington, D.C., American Geophysical Union, p. 87–106.

Singer, B., and Brown, L.L., 2002, The Santa Rosa event: $^{40}Ar/^{39}Ar$ and paleomagnetic results from the Valles rhyolite near Jaramillo Creek, Jemez Mountains, New Mexico: Earth and Planetary Science Letters, v. 197, p. 51–64.

Smith, H.T.U., 1938, Tertiary geology of the Abiquiu quadrangle, New Mexico: Journal of Geology, v. 46, p. 933–965.

Sussman, A.J., Lewis, C.J., Mason, S.N., Geissman, J.W., Schultz-Fellenz, E., Oliva-Urcia, B., and Gardner, J., 2011, Paleomagnetism of the Quaternary Bandelier Tuff: implications for the tectonic evolution of the Española Basin, Rio Grande rift: Lithosphere, v. 3. p. 328–345.

Sussman, A., Lewis, C., Soto, R., and Goteti, R., 2006, Vertical axis rotations associated with relay ramps in the Rio Grande Rift, New Mexico: Geological Society of America, Abstracts with Programs, v. 38, no. 7, p. 417.

Tauxe, L., 1998, Paleomagnetic Principles and Practice: Boston, Kluwer Academic Publishers, 314 p.

Trujillo, R., 2014, Tectonic evolution and magma emplacement of the western Española Basin, New Mexico: a paleomagnetic and anisotropy of magnetic susceptibility study [M.S. thesis]: Las Vegas, New Mexico Highlands University, 83 p.

Wawrzyniec, T.F., Geissman, J.W., Melker, M.D., and Hubbard, M., 2002, Dextral shear along the eastern margin of the Colorado Plateau: a kinematic link between Laramide contraction and Rio Grande rifting (ca. 75–13 Ma): The Journal of Geology, v. 110, p. 305–324.

Wells, R.E., and Hillhouse, J.W., 1989, Paleomagnetism and tectonic rotation of the lower Miocene Peach Springs Tuff–Colorado Plateau, Arizona to Barstow, California: Geological Society of America Bulletin, v. 101, p. 846–863.

Wilson, D., Aster, R., West, M., Ni, J., Grand, S., Gao, W., Baldridge, W.S., Semken, S., and Patel, P., 2005, Lithospheric structure of the Rio Grande rift: Nature, v. 433, p. 851–855.

Wolff, J.A, Rowe, M.C., Teasdale, R., Gardner, J.N., Ramos, F.C., and Heikoop, C.E, 2005, Petrogenesis of pre-caldera mafic lavas, Jemez Mountains volcanic field (New Mexico, USA): Journal of Petrology, v. 46, p. 407–439.

Zijderveld, J.D.A., 1967, A.C. demagnetization of rocks: analysis of results, *in* Collinson, D.W., Creer, K.M., and Runcorn, S.K., eds., Methods in Paleomagnetism: Amsterdam, Elsevier, p. 254–286.